Sialic acids cleavage induced by elastin-derived peptides impairs the interaction between insulin and its receptor in adipocytes 3T3-L1

Alexandre Guillot, Kevin Toussaint, Lucrece Ebersold, Hassan Elbtaouri, Emilie Thiebault, T. Issad, Franck Peretti, Pascal Maurice, Hervé Sartelet, Amar Bennasroune, et al.

Sialic acids cleavage induced by elastin-derived peptides impairs the interaction between insulin and its receptor in adipocytes 3T3-L1

Alexandre Guillot[1,6], Kevin Toussaint[1,6], Lucrece Ebersold[1], Hassan ElBtaouri[1], Emilie Thiebault[1], Tarik Issad[2], Franck Peretti[3], Pascal Maurice[1], Hervé Sartelet[1], Amar Bennasroune[1], Laurent Martiny[1], Manuel Dauchez[1,4], Laurent Duca[1], Vincent Durlach[1,5], Béatrice Romier[1,6], Stéphanie Baud[1,4,6], Sébastien Blaise [1,6,7]

[1] UMR CNRS 7369 MEDyC, University of Reims Champagne-Ardenne, 51100 Reims, France.

[2] Université Paris Cité, Institut Cochin, CNRS, INSERM, 24 Rue du Faubourg Saint-Jacques, 75014, Paris, France.

[3] INSERM, INRAE, C2VN, Aix Marseille University, Marseille, France.

[4] P3M, Multi-Scale Molecular Modeling Platform, Université de Reims Champagne Ardenne, 51097 Reims, France.

[5]Cardiovascular and Thoracic Division, University Hospital of Reims, Reims, France.

[6] Equal contributions

[7] Corresponding author: Sébastien BLAISE, UMR CNRS/URCA 7369, UFR Sciences Exactes et Naturelles, Moulin de la Housse, BP 1039, 51100 Reims, Phone: 03 26 91 34 35 / Fax: 03 26 91 83 66 / ORCID : 0000-0003-3012-1500 / sebastien.blaise@univ-reims.fr

ABSTRACT: The insulin receptor (IR) plays an important role in insulin signal transduction, the defect of which is believed to be the root cause of type 2 diabetes. In 3T3-L1 adipocytes as in other cell types, the mature IR is a heterotetrameric cell surface glycoprotein composed of two α subunits and two β subunits. Our objective in our study, is to understand how the desialylation of N-glycan chains, induced by elastin-derived peptides, plays a major role in the function of the IR. Using the 3T3-L1 adipocyte line, we show that removal of the sialic acid from N-glycan chains (N893 and N908), induced by the elastin receptor complex (ERC) and elastin derived-peptides (EDPs), leads to a decrease in the autophosphorylation activity of the insulin receptor. We demonstrate by molecular dynamics approaches that the absence of sialic acids on one of these two sites is sufficient to generate local and general modifications of the structure of the IR. Biochemical approaches highlight a decrease in the interaction between insulin and its receptor when ERC sialidase activity is induced by EDPs. Therefore, desialylation by EDPs is synonymous with a decrease of IR sensitivity in adipocytes and could thus be a potential source of insulin resistance associated with diabetic conditions.

Key Points: Elastin-derived peptides (EDPs) induce insulin receptor (IR) desialilation. - Sialic acids removed by EDP, change the 3D structure of IR in adipocyte cell line. -The cleavage of sialic acids decreases the affinity between insulin and IR. - EDPs induce an inhibition of IR activity and insulin sensitivity decrease.

Running Title: Sialic acid cleavage decrease the affinity between insulin and its receptor.

Key Words: N-glycan, Insulin receptor, Elastin-derived-peptides, insulin resistance, ligand-receptor affinity

Conflict of Interest: No potential conflicts of interest relevant to this article were reported.

Funding Sources: This work was supported by funding from the CNRS, the University of Reims Champagne Ardenne, Région Grand-Est (OMAGE program, France), University Hospital Federations (Entitled assessment and integrative research on remodeling-inflammation-metabolic stress in systemic and hepatogastrointestinal metabolic diseases, FHU-ARRIMAGE) and European funds FEDER. AG was supported by research grants from the Région

Champagne Ardenne. KT was supported by research grants from URCA. The authors declare no competing financial interests.

ACKNOWLEDGMENTS: We wish to thank Cathy Hachet, Olivier Bocquet and Thinhinane Hocine for technical help. The authors also thank the ROMEO HPC Center, the Multiscale Molecular Modeling Platform (P3M) and the CINES (GENCI grant #c2016077569) for providing CPU-time and support. The authors thank financial and infrastructural support from Chair Modélisation moléculaire et Agroressources: Ingrédients, Cosmétique et Santé, Université de Reims Champagne-Ardenne (MAgICS).

Author's Contributions: *The conception and design of the study* - Alexandre Guillot, Kevin Toussaint, Lucrece Ebersold, Hassan ElBtaouri, Emilie Thiebault, Franck Peretti, Béatrice Romier, Stéphanie Baud, Sébastien Blaise. *The acquisition of data*- Alexandre Guillot, Kevin Toussaint, Lucrece Ebersold, Hassan ElBtaouri, Emilie Thiebault, Franck Peretti, Stéphanie Baud. *Analysis and interpretation of data*- Alexandre Guillot, Kevin Toussaint, Lucrece Ebersold, Hassan ElBtaouri, Emilie Thiebault, Franck Peretti, Béatrice Romier, Stéphanie Baud, Sébastien Blaise. *Drafting the article*- Alexandre Guillot,Hassan ElBtaouri,Béatrice Romier, Stéphanie Baud, Sébastien Blaise. *Critical revision*- Tarik Issad, Franck Peretti, Pascal Maurice, Hervé Sartelet, Amar Bennasroune, Laurent Martiny, Manuel Dauchez, Laurent Duca, Vincent Durlach, Béatrice Romier, Stéphanie Baud, Sébastien Blaise. *Approval of the final version:* All co-authors. The authors declare that all data were generated in-house and that no paper mill was used.

Introduction

Diabetes is a major public health problem affecting all countries of the world, all social classes, and all ages. Thus, in 2021, 537 million people (aged 20 to 79) developed type 2 diabetes[43]. This disease would be responsible for 6.7 million deaths, more than the number of deaths from HIV, tuberculosis, and malaria combined [33, 43]. Various organizations (e.g.: World Health Organization (WHO), international diabetes foundation) agree that the number of diabetic patients should reach 643 million by 2030 and 783 million by 2045[9, 38], suggesting a significant rise in the number of deaths linked to this pathology. Although efforts on management and treatments have multiplied in recent decades, nothing seems to halt this pandemic-like evolution. This could be explained by a notable lack of knowledge of the pathology as well as the cellular and molecular actors implicated. Among these actors, the insulin receptor plays one of the first roles. The insulin receptor (IR) is a membrane protein belonging to the family of receptor tyrosine kinase activity. Initially synthesized as a pro-receptor, IR is formed by 2 α and β subunits, of 130 kDa and 95 kDa, respectively, and linked by a disulphide bridge[10, 37]. While the α subunit is exclusively extracellular, the β subunit contains an extracellular portion of approximately 190 amino acids, a transmembrane helix, and then a cytoplasmic domain of approximately 400 amino acids (supplementary Figure 1). From a functional point of view, the binding of an insulin molecule to the IR causes a conformational modification of the latter. This change brings together the intracellular tyrosine kinase domains of each monomer, thus triggering an autophosphorylation cascade. The tyrosine kinase domain of the IR has indeed many phosphorylation sites. Tyrosines 1158,1162 and 1163 are the first to autophosphorylate and are synonymous with receptor activation. Tyrosines 1328 et 1334 are in turn phosphorylated, then finally tyrosine 972[20, 41, 48]. This last phosphorylation will allow the recruitment and activation of a set of substrates for the insulin receptor. Several complexes signaling pathways will then be set up and lead to different cellular processes such as glucose uptake. Today, the factors described in the literature for the regulation of IR activity are essentially intracellular. Conversely, extracellular factors are poorly described. Among those lasts, extracellular matrix components play a major role. Thus, we have previously described the in vivo impact of Elastin-Derived Peptides (EDPs) on IR without having precisely determined their molecular and structural

effects[6]. EDPs result from the degradation of elastin, found in three main tissues, the skin, the lungs, or the elastic arterial vessels (i.e., aorta, carotids, etc.)[35]. EDPs are, markers of elastic fiber aging whose production is accentuated by inflammatory processes and increased activity of elastases such as metalloproteinases (MMP-2, -7, -9, -12), cathepsins and neutrophil elastase[32, 45]. Interestingly, those proteases are markers of the degree of metabolic syndrome. EDPs harboring a GxxPG consensus motif (where x represents any amino acid) are bioactive because this sequence motif stabilizes a type VIII β-turn conformation. These bioactive EDPs are called elastokines. The typical elastokine is the VGVAPG peptide, a triple repeat sequence encoded by exon 24 of human tropoelastin. Other GxxPG bioactive motifs such as GVYPG, GFGPG or GVLPG and longer elastokines (YTTGKLPYGYGPGG, YGARPGVGVGGIP and PGFGAVPGA) have been reported[12, 32]. These EDPs have been shown to bind to several receptors including the elastin receptor complex (ERC)[42]. This receptor is the most documented and perhaps the most important signaling transducer reported to date. ERC has a unique composition: a 67 kDa peripheral subunit, called elastin-binding protein (EBP), binding EDPs and two membrane proteins, a 55 kDa protective protein/cathepsin A (PPCA) and a 61 kDa neuraminidase (neuraminidase-1, Neu-1)[7, 44]. Neu-1 belongs to the family of mammalian sialidases which are exoglycosidases and essentially catalyzes the hydrolytic cleavage of terminal sialic acid residues carried by N-glycan chains of glycolipids, oligosaccharides, and glycoproteins such as integrins, tyrosine kinase receptors (IR, hepatic (HGFR), epithelial (EGFR), platelet-derived (PDGFR) growth factor receptors), toll-type receptors and platelet glycoprotein Ibs, leading to modulation of receptor activation and signaling[2, 3, 44]. Nevertheless, the molecular consequences of this desialylation on glycoproteins remain poorly understood. The aim of the present study was to describe the impact of desialylation by EDPs and therefore by ERC on the insulin receptor carried by differentiated 3T3-L1 adipocytes which are classically used to study fundamental cellular mechanisms associated with diabetes, obesity and related disorders[22, 25, 30, 39]. Thus, we investigated the effects of EDP on the expression of IR at the cytoplasmic membrane, its endocytosis, its shedding, and the ligand-receptor affinity.

Material and Methods

Cell culture and stimulations: The 3T3-L1 cell line (preadipocytes derived from mouse embryonic fibroblasts also called 3T3) is usually used to study the basic cellular mechanisms associated with diabetes, obesity, and related disorders. 3T3-L1 cells (ATCC) are incubated at 37 °C. in an atmosphere of 5% CO_2, in DMEM medium 4.5 g/L of glucose and containing GlutaMAX® ((Dulbecco's Modified Eagle's Medium, Gibco Thermo Fisher Scientific, France), supplemented with 10% fetal calf serum (Dutscher, France), 1% biotin-panthothenate solution (Sigma-Aldrich, USA), and 1% antibiotic/antimycotic solution (Sigma-Aldrich). To induce differentiation into mature adipocytes, the pre-adipocytes are stimulated for 48 hours post-confluence in the culture medium supplemented with an adipogenic cocktail containing: 3-isobutyl-1-méthylxanthine (IBMX, 0.5 mM, Sigma-Aldrich), dexamethasone (250 nM, Sigma-Aldrich), and insulin from bovine pancreas (10 µg/mL or 1,72 µM, Sigma-Aldrich). Following these 48 hours of incubation with the differentiation cocktail, differentiation is carried out for 9 days by supplementing the DMEM medium with insulin (10 µg/mL). For functional studies (particularly for IR), pre-adipocytes and differentiated (mature) adipocytes are stimulated with insulin (5 µg/mL and 10 µg/mL), EDPs (also called κE, 12.5 µg/ mL to 200 µg/mL), DANA (2-deoxy-2,3-dehybro-N-acetylneuraminic acid, 400µM, Merck)), chondroitin sulphate (200µg/mL, Sigma-Aldrich) and interfering peptides (0.1 µM, GPS 21624 H-ELVDPVVAAGAVVTSSGIVFFSRKR-NH2, see Albrecht et al.). These inhibitors are added 3 hours before the κE treatments. As described in the literature [11] κE is produced from 1 g of insoluble fibrous elastin extracted from bovine neck ligament. Elastin is hydrolyzed in a mixture of ethanolic potash (1 M) in a water bath at 37°C with stirring for 2 h. The supernatant is recovered and cold neutralized with perchloric acid ($HClO_4$) and decanted for 12 hours at 4°C. Ethanol is removed by rotary evaporation at 37°C. The κE solution is dialyzed overnight at 4°C against distilled water with stirring and lyophilized after freezing at -20°C. The κE sequences are verified by HPLC-MS-MS to quantify the sequences in elastin peptides and verify the non-contamination with collagen peptides.

mRNA expression: The total RNAs are extracted using cold trizol (Extract-All, Eurobio) followed by a 24:1 chloroform/isoamyl alcohol mix. After centrifugation (12,000 g, 15 min, 4°C) and washing with chloroform, an equivalent volume of isopropanol is added to the aqueous phase for the precipitation of the RNAs. Once centrifuged, washed with ethanol (75%) and dried, RNAs are resuspended in water. The purity and quality of the extracted RNAs are analyzed by spectroscopy and migration on a 1% agarose gel. 250 ng of RNA is treated

with DNase and reverse transcription is performed using the RT kit (Abgene ThermoScientific). RNAs are stored at -80°C and cDNAs at -20°C. 5 µl of a 1/10th dilution of cDNA is used for qPCR analysis. The cDNAs are added to the mix containing 7.5 µl of SYBRGreen (ThermoScientific), 1.4 µl of primers (250 nM) and 1.1 µl of water. The fluorescence is measured by the qPCR CFX96 device (BioRad). The melting-curves and the Ct (cycle threshold) are validated for each repetition and the results are normalized according to the housekeeping gene RPS26.

Protein extractions and Western Blot: *For total protein extraction*, the cells are lysed (at 4°C) in RIPA buffer (Triton X-100 1% (v/v); Na-deoxycholate 1% (w/v); Sodium dodecyl sulfate 0, 1% (SDS, w/v); 20 mM Tris pH 7.5; 150 mM NaCl, 1 mM DTT, 1 mM sodium fluoride, 1% protease inhibitor cocktail (Sigma-Aldrich), 1 mM orthovanadate). After centrifugation (20,000 g, 30 min, 4 °C.), the supernatant is recovered, and the proteins contained are assayed using the BCA kit (Interchim, France). *For membrane extraction,* membrane extraction buffer (SEM: 75 mM Tris; 2 mM EDTA; 12 mM $MgCl_2$) is added to the cells. The cells are scraped and recovered before being sonicated allowing the opening of the membranes. The samples are then centrifuged (20,000 g, 45 min, 4°C) to pellet the membranes and eliminate the cytosolic proteins. The supernatant is stored at -20°C for possible cytosolic protein analysis. The membrane pellet is suspended in SEM using a syringe and needle. A detergent is then added (Triton-X100, 10 µl for 100 µl of BEM) to solubilize the membrane proteins. The lysate incubates for 3 h at 4°C on a wheel. Insoluble debris are removed by centrifugation (20,000 g, 30 min, 4°C), and the supernatant is collected and stored at -20°C before analysis, if necessary. A BCA protein assay is also performed. *Western blot:* The samples are subjected to Laemmli denaturing buffer (50 mM Tris HCl pH 6.8, 10% (v/v) glycerol, 0.001% (w/v) bromophenol blue, 2% (w/v) SDS, 20% (v/v) β-mercaptoethanol), and heated (10 min at 100°C). 80 µg of proteins are deposited on a polyacrylamide gel (8%), under denaturing and reducing conditions (SDS-PAGE). Migration takes place in migration buffer (0.02 M Tris Base, 0.2 M Glycine, 0.1% (w/v) SDS). Protein transfer onto a nitrocellulose membrane (Whatman Protran) is carried out in buffer containing 20% (v/v) ethanol, 25 mM Tris, 192 mM glycine. After saturation, the membranes are incubated overnight at 4°C with anti-insulin receptor (1/1000, cell signaling, 3020S), anti-phopho-insulin receptor (1/1000, AbCam, ab5678), anti-actin (1/2000, Santa cruz biotechnology, sc-47778) antibodies previously diluted in TBS-T buffer (50 mM Tris-HCl pH 7.5; 150 mM NaCl; 0.1% (v/v) Tween 20 (polysorbate) and 5% BSA (bovine serum albumin, w/v).

Secondary antibodies are coupled with horseradish peroxidase (HRP). The proteins labeled by Horseradish peroxidase (HRP)-linked secondary antibodies are revealed by chemiluminescence (Amersham ECL Western Blotting Detection Reagents kit, GE Healthcare). Revelation and quantification are done using the Odyssey device from Li-Cor.

Immunoprecipitation of protein and sialic acid detection: In order to evaluate the protein partners of the RI, immunoprecipitation is performed. For immunoprecipitation, 400 µg of proteins (extracted in the absence of SDS) are immunoprecipitated with 3 µl of anti-IR antibodies / PBS (12 h, 4°C) then with 40 µl of protein G sepharose (GE Healthcare) / PBS (4 hrs, 4°C). After washing and centrifugation (2 min, 10,000 g), the pellet is kept for analysis by western blot. The proteins are suspended in Laemmli denaturing buffer (50 mM Tris HCl pH 6.8, 10% (v/v) glycerol, 0.001% (w/v) bromophenol blue, 2% (w/v) SDS, 20% (v/v) β-mercaptoethanol), heated (10 min at 100°C) and centrifuged (10,000 g, 30 s). The supernatant is then placed on a polyacrylamide gel for analysis by western blot. The quantification of sialic acids is done with the DIG Glycan Differentiation kit (Roche), after the transfer operation. This kit allows the recognition of sialic acids using lectins coupled to digoxygenin. A final anti-digoxygenin antibody coupled with an alkaline phosphatase allows labeling to be carried out.

IR endocytosis assay: The cells are washed twice with cold PBS, on ice. They then undergo a biotinylation step on ice to label all the membrane proteins: 30 min of sulfo-NHS-LC-Biotin (ThermoFisher Scientific) at 0.5 mg/mL in phosphate-buffered saline (PBS) on ice, 3 PBS rinses, 15 min of 100 mM glycine in PBS, then 3 PBS rinses. The cells are then returned for 15 min in the incubator in the presence of medium preheated at 37°C ± 100 nM insulin. This step makes it possible to relaunch the phenomena of endocytosis and thus to internalize the previously biotinylated proteins. The cells are then returned to the cold in order to stop endocytosis. After a PBS wash, a 10 min treatment with 1 mg/mL pronase in cold PBS degrades the biotinylated proteins that have not been internalized. A positive control is performed by skipping this degradation step (recovery of all the biotinylated proteins). The cells are then suspended and centrifuged for 10 min at 1000 RPM and at 4°C, in order to eliminate the supernatant. The cells are then lysed (according to the protocol described previously) and assayed (BCA assay). 500 µg of proteins are incubated with 40 µl of avidin-agarose beads (ThermoFisher Scientific) overnight. After several rinses of the beads with the lysis buffer, the

proteins are detached from the beads by denaturation (Laemmli and heating at 100° C. for 10 min). After centrifugation, the proteins contained in the supernatant are placed on a gel for analysis by western blot.

Shedding of IR: This experiment makes it possible to study the degradation of the extracellular fragments of membrane proteins. By using DAPT (N-[N-(3,5-Difluorophenacetyl)-L-alanyl]-S-phenylglycine t-butyl ester), the c-terminal fragments of the cleaved forms of the protein of interest are retained, thus facilitating their detection. The shedding of the IR is evaluated on the 3T3-L1, ± treatment with DAPT at 10 µM for 15 h. The quantity of the c-terminal fragment of the IR is then measured by western blot.

Glucose uptake: Glucose uptake is measured using tritiated 2-deoxy-D-glucose (PerkinElmer). The cells (12-well plate) are washed with Krebs-Ringer phosphate buffer (KRP buffer, 10 mM KH2PO4 pH 7.4; 136 mM NaCl; 4.7 mM KCl; 1.25 mM $CaCl_2$; 1.25 mM $MgSO_4$; 0.05% (p (v) bovine serum albumin). They are then incubated for 30 min at 37°C with KRP buffer with or without 100 nM insulin (basal or stimulated assimilation), then 5 min at 37°C with KRP buffer ± insulin and containing 100 µM of 2-deoxy-D-glucose (non-radiolabelled, Sigma Aldrich) + 0.2 µCi/mL of tritiated 2-deoxy-D-glucose (radiolabelled). The cells are then washed 3 times with cold PBS and then dissolved in 500 µl of a 0.1 M NaOH solution. 200 µl of the sample are then added to 4 mL of scintillating product and counting is carried out over 10 min per sample. At the same time, part of the rest of the sample is analyzed by BCA assay to standardize the results obtained by counting.

Affinity ligand-receptor: In order to evaluate the interaction between the insulin and its receptor in the presence or absence of EDPs, we incubated the cells (80% confluence) for 24 hours with increasing concentrations of κE (0 to 200 µg/mL). Then, adipocytes are incubated for 30 minutes with insulin-FITC (5/6-fluorescein isothiocyanate) at different concentrations (from 0 to 1.72 µM). After several washes to eliminate free insulin, the amount of fluorescence of the bound insulin-FITC is measured (Life science, Switzerland). A normalization of the fluorescence of bound insulin was done, in function to the quantity of proteins (BCA assay) or the number of cells. Thus, the cells are quantified by adding Hoechst reagent (10 µg/mL, 5

minutes) to the wells and then visualizing the number of cells using the EVOS® FL Auto device (Thermo Fisher Scientific, Massachusetts, United States -United). Counting is done by ImageJ. The representation of Dixon (1/insulin-FITC fixed according to the concentrations of κE) allows the determination of the constant of inhibition (Ki) of the κE and the secondary graph (1/insulin-FITC fixed according to 1/insulin total) allows the determination of the dissociation constant (KD) between insulin and its receptor.

Molecular modeling: *Molecular docking simulation* - Molecular docking simulation is performed between the ectodomain dimer of IR and Neu-1. The
IR dimer structure was setup using the crystallographic data of the 3LOH entry of the PDB (Protein Data Bank). The structure of Neu-1 comes from a previous study and has been obtained using homology modeling performed with bacterial neuraminidase (PDB entry 1EUR) as a template. Rigid protein/protein molecular docking simulations are performed using Hex 8.0.0 software. Sampling of the possible conformations is done thanks to the rotation of the ligand (Neu-1) on itself, as well as by the rotation of the ligand around the target (IR dimer). The search is based on Fourier spherical polar correlations which accelerates the calculations. In addition, since the IR dimer is a large molecule, the search on its surface is performed using 62 spheres with a radius equal to 15 Å. The parameters used during the simulation are summarized in Table 1. For each docking pose, an energy score is calculated. *Molecular dynamics simulations* - As described previously, the structure of the dimer of the ectodomain of the IR is assembled from the PDB structure having as reference 3LOH. All N-glycosylation chain structures are constructed using Avogadro software. Each block of the glycan is constructed separately and subjected to an energy minimization step. The chain is then assembled block by block with energy minimization at each step until the complete structure of the glycan is obtained. A modified version of the OPLS-AA (Optimized Potentials for Liquid Simulations – All Atom) force field is used to describe these atoms[15]. For simulations including the IR, the asparagines of the glycosylated chains are aligned with the asparagines of the targeted sites on the protein (N893 or N906), then the chains are oriented towards the outside of the protein to avoid the steric clashes. In order to simulate the anchoring to the membrane of the receptor, the last 3 residues of the C-terminal end are immobilized by applying strong force constraints to them. The molecular dynamics (MD) simulations are carried out using the OCCIGEN supercomputer from CINES and the GROMACS software

(package 5.0.2). Before each production run, the system is subjected to several preparation steps. First, the potential energy of the system is minimized in vacuum over 2,500 iterations (steepest descent energy minimization). Periodic boundary conditions are applied by generating a cubic box around the structures. This box is then filled with water molecules (TIP3P, explicit water model), followed by 2,500 iterations of energy minimization in the solvent. Finally, 500 ps equilibration (NPT conditions) is performed to bring the system to the desired pressure and temperature (1 bar and 310 K, respectively) and to allow the solvent molecules to relax around the protein that is immobilized. Table 2 summarizes the parameters used for the 250 ns NPT molecular dynamics simulations. Atomic coordinates are recorded every picosecond and the LINCS algorithm is used to freeze bonds involving a hydrogen atom (2 fs integration time step). Each system is simulated at a physiological temperature of 310 K. The analysis of the trajectories is carried out from the reduced trajectory files, with a temporal resolution of 10 ps (100 ps for the cluster search). All visualizations are produced using Visual Molecular Dynamics (VMD) software and Tachyon rendering mode.

Statistical analyzes: The results are expressed as the mean ± standard deviation. An ANOVA test was performed to compare the results obtained. The results are considered statistically significant when the threshold $p < 0.05$ is reached (* $p < 0.05$; ** $p < 0.01$; *** $p < 0.001$).

Results

Insulin receptor desensitization by ERC activation.

In order to study the impact of short or prolonged stimulation of EDPs on the activation of the IR, we treated pre-adipocyte fibroblasts 3T3-L1 undifferentiated or differentiated into mature adipocytes with κ-elastin (κE). Previously, Blaise et al. described that κE has a biological composition very similar to a mixture of EDPs resulting from enzymatic hydrolysis. A κE concentration of 50 µg/mL was used, with variable incubation times from 1 to 24 h. By western-blot, we evaluated the autophosphorylation capacity of tyrosine 972 of the IR following stimulation with insulin (100 nM, for 30 minutes). In preadipocytes or mature adipocytes (Figure 1A), short duration κE treatments failed to induce significant changes in the sensitivity of IR to its ligand. On the other hand, prolonged stimulation of κE (24 h) makes it possible to reduce by almost half the ratio between phosphorylated IR and total IR. Regardless of the duration of exposure to EDPs, the basal phosphorylation (without insulin stimulation)

level of the receptor is not impacted and remains stable. Comparable results were also obtained on the phosphorylation of tyrosine 1163, earlier in the receptor activation process (Data not shown). Finally, the ratio between IR and actin remains stable, suggesting that κE does not modify the level of expression of the receptor, but causes a dysfunction of the latter. Figure 1B shows, by simulations of molecular docking carried out between the subunit Neu-1 of the ERC and the IR an interaction between these two partners. Docking simulations allow the identification of two sites of interactions. The first one is located on the α chain of the IR, at the interface between the cysteine (C) and leucine 1 and 2 domains (L1 and L2). The second one is located on the β chain of the IR, closer to the plasma membrane, at the level of the fibronectin 3 (Fn3) domain and extends slightly over the fibronectin 2 (Fn2) domain. In order to confirm this interaction between Neu-1 and IR, we immunoprecipitated the IR and, by western blot, we evaluated the level of co-immunoprecipitation of the Neu-1, level of phosphorylation of the IR, as well as the level of sialic acids at the IR and target of Neu-1 in preadipocytes (Figure 1C) and mature adipocytes (Figure 1D). We thus show that there is a correlation between these 3 parameters. The EDPs cause an interaction between the IR and Neu-1 which will play its role of sialidase by hydrolyzing the sialic acids present on the surface of the IR. Finally, we incubated the cells before κE stimulation, with two ERC inhibitors: chondroitin sulfate (CS) which acts as a competitive inhibitor of EBP; and DANA (2-deoxy-2,3-didehydro-N-acetylneuraminic acid) which is an inhibitor of the activity of sialidases such as Neuraminidase-1 (Neu-1). These inhibitors reversed the effects on the insulin receptor induced by EDPs. Figure 1F showed that desialylation of the receptor, unlike its phosphorylation, was independent of insulin stimulation. These first results suggested that the reduction in the phosphorylation activity of IR is indeed dependent on insulin, as well as on the degree of sialylation of RI, whether in pre-adipocytes or mature adipocytes. Finally, supplementary Figure 2 shows that after 8 weeks of administration, the presence of EDP (kE: 10 µg/kg or 100 µg/kg as described in [32]) promotes hyperglycemia associated with glucose intolerance and insulin resistance. Conversely, we administered treatments to obese and diabetic mice (Db/Db aged 8 weeks) to block the effects of EDPs generated by the inflammatory status of the model. Thus, the use of a neutrophil elastase inhibitor (GW311616A, 2 mg/kg per day for 14 days as described in [40]), or ERC inhibitors such as DANA (10 g/L per week for 8 weeks as described in [8])), or CS (50 mg/kg per week for 8 weeks as described in all significantly reduced hyperglycemia, glucose intolerance, and insulin resistance in these

animals. These in vivo data confirm the in vitro data demonstrating that EDPs play a major role in the insulin resistance of cells and tissues.

Desialylation induced by EDPs does not affect expression, endocytosis or shedding of insulin receptor

After determining that the IR activity of 3T3-L1 differentiated or not, could be inhibited by EDPs, we investigated how sialic acids removed by Neu-1 affect IR activity. As illustrated in Figure 1, elastin peptides do not appear to be responsible for modifying IR expression. This hypothesis is confirmed by a qPCR analysis of the level of mRNA of IR present in the preadipocytes after treatments with κE (Figure 2A). This analysis did not detect any changes in the expression level of the insulin receptor. According to the results presented in Figure 2B expression of IR proreceptor is also not impacted by κE treatments. Poor membrane localization of the IR could also have explained the differences in phosphorylation levels following stimulation with EDPs. For this reason, we have produced extracts of membrane proteins: the adipocytes undergo 2 stages of lysis, a first without Triton-X100 makes it possible to separate the cytosolic proteins without dissolving the membranes. A second step, with Triton-X100, makes it possible to solubilize the remaining membrane proteins. The analysis of membrane protein extracts by western blot does not indicate any variation either of the IR or pro-IR forms and suggests that the EDPs do not modify the localization of the IR at the membrane (Figure 2B).

Upon activation, the IR is internalized in the adipocyte, and then can be recycled several time at the plasma membrane. We therefore evaluated the endocytosis capacity of the IR in order to detect either early endocytosis (independent of insulin stimulation) or excessive recycling after stimulation. The endocytosis test is done in several steps as described by Theret et al. The proteins at the adipocyte surface are biotinylated, then the cells are returned at 37°C to restart the endocytosis process (± insulin). Finally, treatment with a cocktail of proteolytic enzymes (proteases) eliminates biotinylated proteins that have not been internalized. Internalized and biotinylated proteins are recovered by precipitation with avidin beads. A positive control is also carried out by skipping the protease treatment step (all the biotinylated proteins are therefore recovered). Our results indicate that κE does not appear to induce internalization of IR in the absence of insulin stimulation (Figure 2C, left panel). Insulin causes IR phosphorylation, as well as its endocytosis at the level of the positive control (Figure 2C, right panels). In addition, κE causes a 2-fold decrease in both endocytosis and receptor

phosphorylation. On the other hand, the ratio between endocytosed IR and its phosphorylated form remains stable. This information indicates that the decrease in the amount of internalized IR is attributable to the decrease in receptor activation, observed previously. According to these elements, EDPs do not seem to be able to directly modulate IR endocytosis, independently of its phosphorylation.

Finally, we evaluated shedding of IR, a process during which the extracellular part of a receptor is cleaved and released into the extracellular environment. Because this mechanism is regularly found in diabetic patient, a study of IR shedding after treatment with κE was therefore performed (Figure 2D). Under suitable conditions, the soluble part of the IR (IR-s) can be assayed by Elisa test to evaluate the shedding of the receptor. However, since this fragment is present in quantities too small to be assayed, it was preferred to assess the amount of IR C-terminal fragments (IR-ctf) by Western blot. In addition, since this fragment is normally rapidly degraded by γ-secretases, the use of DAPT (γ-secretase inhibitor) makes it possible to accumulate the IR-ctf and facilitate its detection. As illustrated in Figure 2D, the amount of IR-ctf found does not seem to vary with EDP treatment, regardless of whether or not DAPT is used. It therefore appears that EDPs do not accelerate IR shedding.

Desialylation induced by EDPs affects the affinity between insulin and its receptor.

Because EDPs do not affect IR trafficking to the membrane, we hypothesized that the sialic acids removed by EDPs could influence the ~~role~~ binding of insulin to its receptor. Thus, we performed a kinetic study of IR stimulation by modulating the incubation time of insulin (at constant concentration) with adipocyte cells in the presence or absence of κE (Figure 3A). In conditions without κE, we demonstrated that one hour of stimulation, phosphorylation is maximal before decreasing after 10 hours of incubation (which might be explained by endocytosis phenomenon). When the adipocytes are previously incubated with κE (50 µM for 24 hours), the maximum phosphorylation is only reached after 6 hours of insulin stimulation. After 10 hours of stimulation, IR phosphorylation is still maximal. On the other hand, after 24 h of stimulation, the phosphorylation levels are similar between cells treated or not with κE. These data therefore suggest that the interaction of the insulin receptor with its ligand may be reduced when the glycan chains of IR lose sialic acids by EDP. To confirm our hypothesis, we measured the affinity of insulin with its receptor and its modulation in the presence of EDPs. First, we incubated the cells for 30 min with increasing concentrations of fluorochrome

FITC-labeled insulin (6.88, 13.78 and 20.66 10^{-6} M) in the presence or absence of κE (25 and 50 $\mu g.mL^{-1}$) and measured the fraction of insulin bound to the cells (Figure 3B). The results showed that insulin interaction with IR has a constant K_D of about 6.89 10^{-6} M. The presence of κE increased the K_D value to 33.33 and 66.66 10^{-6} M with 25 and 50 $\mu g.mL^{-1}$ respectively. However, the maximal insulin-binding was not affected. These data suggested that κE reduced the affinity of insulin to its receptor. In a second step, we evaluated the dose effect of κE on the interaction of insulin with its receptor using the Dixon method. We incubated the cells for 24 hours with κE (25 and 50 $\mu g.mL^{-1}$) in the presence or absence of fluorochrome FITC-labeled insulin (6.88, 13.78 and 20.66 10^{-6} M, for 30 minutes) and measured the fraction of insulin bound to the cells (Figure 3C). The obtained results confirmed that κE affected the affinity between insulin and IR since the Dixon lines crossed above the x-axis with a K_I of κE in the order of 6.9 $\mu g.mL^{-1}$. We have recently showed that κE binding to EBP leads to Neu-1 activation and induction of its sialidase activity[6, 21, 31]. To confirm Neu-1 involvement in the modulation of IR affinity by κE, we incubated the cells for 30 min with increasing concentrations of fluorochrome FITC-labeled insulin (6.88, 13.78 and 20.66 10^{-6} M) in the presence or absence of Bacterial neuraminidase (0.1 and 0.2 $\mu g.mL^{-1}$) and measured the fraction of insulin bound to the cells. Figure 3D and supplemental data 3 showed that Bacterial neuraminidase also reduced the affinity of insulin to IR. Indeed, we observed an increase of K_D value to 16.8 and 71.9 10^{-6} M with 0.1 and 0.2 $\mu g.mL^{-1}$ respectively. When cells are incubated simultaneously with κE and the sialidase inhibitor DANA, an increase in fluorescence was observed, but without returning to basal levels (Figure 3E). This result confirmed that the reduction of affinity between insulin and IR induced by κE is dependent on the sialidase activity. However, and surprisingly, when these adipocytes are treated with the interfering peptide (PepNat), specific inhibitor of Neu-1[1], in parallel with κE (Figure 3E), we observe a drop in cellular fluorescence. This would seem to indicate that specific inhibition of Neu-1 activity potentiates the effects observed with κE alone, in other word, accentuates the drop in the interaction of insulin with its receptor. This therefore suggests that sialic acid withdrawals on N-glycan chains are major elements in the regulation of IR activity.

The desialiation of N-glycan chains locally affects the areas covering the insulin receptor.

The investigation of the molecular interactions (Figure 1B) between Neu-1 and the insulin receptor through molecular docking highlighted two potential binding sites; we thus assumed that modifications of the N-glycan chains at position N893 and N906 could be responsible for the decrease of affinity between IR and insulin. Indeed, these two asparagine residues are in sequence relevant to N-glycosylation and are the closest of the potential binding sites. First, the local consequences on the structure of the insulin receptor, upon removal of sialic acids on N-glycan chains (Ng-cs) were determined using *in silico* experiments. During initialization of the molecular dynamic simulations, the Ng-cs are placed perpendicular to the IR surface to avoid any steric clashes or entanglements in the protein. At the start of the simulation, the interactions between protein and glycan are therefore reduced to a minimum. However, very quickly (a few nanoseconds), the glycan comes into contact with the protein, suggesting an interaction with the latter. By measuring a proximity score between each residue of the protein and each block of the glycan throughout the simulation, it is possible to identify the areas of interaction between these two partners. On the N893 site (FIG. 4A), the Ng-c2Sf (the biantennary sialylated and fucosylated chain) approaches only the residues belonging to the fibronectin 3 domain, and more particularly the residues close to the membrane (residues 910 to 915 for example).

In contrast, the glycan linked to the N906 site (Figure 4B) interacts with a much wider range of amino acids, belonging to 4 different domains (leucine 1, cysteine, and fibronectin 2 and 3). At the N893 site, the glycan wraps around the F915 residue and places itself in the pocket formed by the S896, E911 and T913 residues (Figure 4C panel i), with the SA facing the interior of the protein. On the N906 site (Figure 5C panel i), the chain fits into a larger pocket, located at the intersection of the leucine, cysteine and fibronectin domains of the IR. Here also, the SA are directed towards the interior of the cavities. Desialylation of Ng-c from the N893 site leads to a slight modification of the residues involved in the glycan/protein interaction. The desialylated glycan interacts with protein residues even closer to the membrane (915-920, Figure 4A). Moreover, for this same site, the area under the curve decreases by about 40% upon desialylation, indicating a lower proximity score, and therefore a greater distance of the chain from the IR. This greater distance is also observable in Figure 4C (panel ii), where the desialylated glycan is arranged almost perpendicular to the IR and no longer fits into the previously identified cavity. Cleavage of SA from the N906 site causes markedly different effects. In this case, desialylation causes significant changes at the level of the residues of the

IR involved in the interaction with the glycan (Figure 4B): reduction of certain interactions as with residues 185-195, and appearance of new interactions (residues 610-630, for example). This suggests that the chain is capable of integrating into a new, hitherto unexplored pocket. On the other hand, upon desialylation the area under the curve remains relatively stable, indicating that, overall, the glycan maintains a position close to the protein. Indeed, as ilustrated in Figure 4D (panel iii), the glycan moves away from the cysteine domain and integrates a new pocket further inside the fibronectin 2 domain. From these results, it therefore appears that the desialylation of glycans can lead to a significant modification of its interaction with the IR. It can cause the glycan to both leave its original pocket and decrease its interactions with the protein (site N893), or just lead to a simple change between 2 possible positions in contact with the IR (site N906). These modifications of interactions are also accompanied by a change in the explored conformations of the glycan such as “broken-wing” or “bird” conformations ~~(see Guillot et al. [15]).~~ The non-occupancy of those several pockets by the N-glycan chains (without sialic acids) could suggest a potential docking with other proteins regulating thus, IR function.

Desialylation of N-glycan chains affects the general conformation of the insulin receptor.

As it has been previously demonstrated that the removal of sialic acids on N-glycan chains locally modulates IR structures, the possible impact of the absence of sialic acid on glycosylation chain on the general structure of the dimer IR was explored. To assess the impact of the presence of Ng-c, a simulation of the protein dimer without any glycosylation chain was also included (Control, Figure 5, IR alone). Progressively, and regardless of the state of glycosylation (with or without SA), the IR is subjected to slow but wide-ranging motions. Thus, at the end of the different simulations, the structure of the receptor is more or less strongly modified compared to the initial structure. These changes are reflected in several ways: a "collapse" of the dimer, visible on the IR carrying the Ng-c2Sf on the N906 site (labelled IR Ng-c2Sf N906); a notable loss of the symmetry of the two monomers, particularly observable on the IR Ng-c2f N893; or a twist around the vertical axis in the case of the IR Ng-c2f N906 system. From the results obtained, it also seems that the main points of IR flexibility lie between the different domains, linked together by a single peptide segment. Indeed, the domains that are formed from an intertwining of the peptide chain adopt highly ordered secondary structure and thus demonstrate greater stability. Regardless of the glycosylation site involved, the

structure of the IR appears to be modified after removal of the SA. These data suggest that chain desialylation is capable not only of modifying the structure of the glycan involved and its interaction network with the protein surface, but also of impacting the entire structure of the IR. Although IR motions are relatively slow, they may be sufficient to explain a decrease in affinity between insulin and IR.

Discussion

In the context of an exponential evolution of diabetes, understanding the mechanisms leading to the loss of sensitivity of the IR is a major axis of research in endocrinology in order to develop new therapeutic leads. This study demonstrates that the accumulation of EDPs generated by aging [4, 23] or tissue inflammation (skin, lung, elastic vessels) due to obesity or diabetes [28, 29, 31, 32], is responsible for a decrease in the phosphorylation activity of IR in pre-adipocyte or mature adipocyte cells and could, partly explain the adipogenesis decrease observed in several *in vitro* or *in vivo* studies[6, 19, 39]. This decrease in IR activity leads to a decrease in associated signaling pathways such as a decrease in glucose uptake, which then promotes hyperglycemia with its known deleterious consequences on the organism.

Bioactive EDPs, also called elastokines, mediate several biological effects through their binding to a singular cell surface receptor called the elastin receptor complex (ERC)[5]. ERC is a heterotrimer composed of a peripheral subunit, (EBP), binding EDPs, a protective protein or cathepsin A (PPCA) and transmembrane neuraminidase-1 (NEU-1) with sialidase activity[42, 44]. It is important to note that the coding sequence for EBP corresponds to an alternative splicing of the coding sequence for beta-galactosidase (B-Gal) on the one hand[7], and that the PPCA/Neu-1 complex[44] is involved in both the ERC and also in the lysosome complex. Therefore, the identification of ERC in biological phenomena remains complex since the use of siRNA against EBP would also lead to B-Gal inactivation, and total Neu-1 silencing would compromise the lysosomal function and consequently cell survival. This is why we used pharmacological treatments (chondroitin sulphate and DANA) in order to block the binding of EDPs to EBP or partially block Neu-1 activity, respectively[44, 46]. Thus, the use of those molecules has shown us that the ERC is involved in the activity of IR in pre-adipocytes and in mature adipocytes. As we show by immunoprecipitation completed with modeling approaches, the Neu-1 subunit interacts with the leucine- and cysteine-rich domains (L1, L2, and C) of the IR. Knowing that NEU-1 is a membrane protein [24] on the one hand and on the

other hand that the L1, L2 and C domains are quite far from the membrane, it is unlikely that this interaction can take place here. On the other hand, the second interaction observed by modeling between Neu-1 and the fibronectin domains (Fn2 and Fn3) of the IR (beta chain) is more probable because it is situated closer to the cell membrane. Moreover, supplemental figure 1 shows that those fibronectin domains have two glycosylation sites (N893 and N906) and protein/protein docking results identify them as preferred targets of the Neu-1 subunit. Thus, through its sialidase activity, Neu-1 can easily cleave the terminal sialic acids of the N-glycan chains. Desialylation of one or both N-glycans (N893 and N906) could then be sufficient to decrease the level of IR phosphorylation. But how can one explain then that a simple loss of sialic acids on one or two N-glycan chains can induce receptor inactivation? We investigated several biochemical approaches to try to explain this loss of function. We demonstrate that desialylation induced by EDPs affect the affinity between IR and insulin. Nevertheless, molecular aspects leading to the desialylation of N-glycan chain such as N893 and/or N903 to ligand-receptor affinity, remain unknown. The molecular dynamics simulations that we have used are currently the only method capable of unraveling at the atomic level the specific impact of each glycosylation chain on the protein. Our data suppose that the variations in the position of the different constituent sugars of the structure of the N-glycans attached to the IR compared to the isolated N-glycans[15], are not obtained randomly but could depend on the protein environment with which N-glycans interact The absence of sialic acids causes a decrease in the "broken wing" conformation of the N-glycan chains, in favor to the "bird" conformation, indicating an opening of the N-glycan antennae[15]. At the same time, the mobility and the number of intermediate structures also increase, in agreement with Guillot et al[15]. Concerning the interactions between the glycans and the different residues of the IR, the trajectories obtained indicate that the glycan, initially positioned perpendicularly to the protein surface, folds up entirely along the protein. By calculating the proximity score between the different IR residues and the glycan chain, it is possible to identify the residues that are most involved in this interaction. The N-glycan situated on N893 interacts with a few residues, all belonging to the fibronectin 3 domain of IR. On the other hand, the N-glycan situated on N906 requisitions more amino acids in its interactions, and they belong to 4 different domains of the IR (domains leucine 1, cysteine, and fibronectin 2 and 3) (supplementary Figure 1). The cleavage of sialic acids from these chains also produces different effects, depending on the site where the glycan chain is placed. On the N893 site, a shift of the glycan chain is observed

towards residues closer to the membrane, as well as an overall distancing of the glycan from the protein (the N-glycan chain rises from the protein surface and does not remain elongated along the IR). On the N906 site, the glycan chain remains in close contact with the protein, but the residues involved in the interaction are more strongly modified: a reduction in the proximity score associated to residues of the cysteine domain is observed, in favor to residues belonging to the fibronectin 2 and 3 (supplementary Figure 1). 3D observation of the conformation of the glycan and the IR confirms these elements. At site N893, the absence of sialic acids allows the glycan to detach from the IR surface and thus come in the vicinity and interact with residues closer to the membrane. At the N906 site, the glycan is inserted into a deep pocket, at the interface between several IR domains, thus explaining the greater variety of residues involved in its interaction with the IR. Removal of the sialic acids causes the glycan to leave this pocket and integrate into a second, adjacent cavity. This displacement of the glycosylation chain from one pocket to another could facilitate the interaction of IR with other extracellular or transmembrane protein partners. In addition to characterizing the local effects of desialylation, the more general impact of this process on IR structure was investigated. To this end, the structure of the dimer of the IR ectodomain was assembled from the PDB structure with reference 3LOH. It was thus demonstrated that, along the MD simulations, the IR is subjected, during the simulation, to slow but large- amplitude movements. Moreover, depending on the glycosylated sites (N893 and N906), and on the presence or absence of sialic acids, the IR adopts different motions such as rotations, twists or collapses. These motions could therefore be due to local variations in the structure of glycan chains generated by the desialylation described above. Thus, the loss of interaction between the glycan situated on N893 and the L1, C and L2 domains could compromise the stability of the IR and cause the collapse of the IR (supplementary Figure 1). These leucine- and cysteine-rich domains are the insulin interacting regions. It seems reasonable to assume that the destabilization of these L1, C and L2 domains could modify the interaction between the receptor and its ligand. Indeed, the binding of insulin to the alpha subunits triggers a conformational change on the beta subunits, an auto-trans-phosphorylation of the tyrosine kinase domains of the IR. There are two distinct interface insulin binding sites on IR, the molecular details of insulin binding to IR remain poorly understood. Insulin binds primarily to the C-terminus of the α chain, (αCT) of one half of the IR dimer; this binding moves the C-terminal β strand (of the insulin B chain) away from the insulin core. The second insulin binding site consists of the loops at the junction

of the Fn1 and Fn2 domains in the other half of the dimer. How insulin binds to its binding site 2 remains largely unknown and may require conformational changes that move the Fn1 and Fn2 domains away from the L1 and CR domains. The rotations and collapse induced by the loss of sialic acids could limit insulin binding both sites. This drop in affinity that can be inferred by modeling approaches has been confirmed by biochemical approaches. Thus, it was demonstrated that the loss of sialic acids either by bacterial neuraminidase or via EDPs leads to a decrease in the insulin-IR interaction. Thus, EDPs have a significant inhibition constant around 20 µg/mL and induce a significant increase in the dissociation constant compared with the basal level. The loss of sialic acids by the EDPs is explained by the sialidase activity of the ERC, with regard to the use of the DANA inhibitor. However, DANA is an inhibitor of neuraminidase 1 and 3 (Neu-3) at the level of the cytoplasmic membrane[16]. Surprisingly, the use of PepNat, a specific Neu-1 inhibitor, seems to reduce the insulin-IR interaction even more than the addition of EDP. This assumes that Neu-3 could be brought into play upon activation of the ERC. The involvement of Neu-3 in the regulation of metabolism has been widely described, particularly in the induction of insulin resistance[34, 47]. Nevertheless, it will be necessary in future studies to take Neu-3 into account in the Neu-1 activation process. This remark is all the more important since the studies of Pshezhetsky's team [13, 14] showed that the deficit of Neu-1 is responsible for insulin resistance. However, in these studies, Neu-1 is not integrated into the ERC and stimulated by EDPs.

In conclusion, this study has therefore demonstrated that EDPs, through ERC activation, induce a decrease in the IR activity both in pre-adipocytes and mature adipocytes. The loss of sialic acids caused by EDPs induces a decrease in the affinity between insulin and IR. The use of inhibitors of the activity of the neuraminidase subunit makes it possible to limit this decrease and could then be an interesting therapeutic avenue to limit the action of EDPs in the induction and/or progression of diabetes in the patient.

REFERENCES:

1. Albrecht C, Appert-Collin A, Bagnard D, Blaise S, Romier-Crouzet B, Efremov R G, Sartelet H, Duca L, Maurice P and Bennasroune A, (2020) Transmembrane Peptides as Inhibitors of Protein-Protein Interactions: An Efficient Strategy to Target Cancer Cells?, Front Oncol 10 519.

2. Amith S R, Jayanth P, Franchuk S, Finlay T, Seyrantepe V, Beyaert R, Pshezhetsky A V and Szewczuk M R, (2010) Neu1 desialylation of sialyl alpha-2,3-linked beta-galactosyl residues of TOLL-like receptor 4 is essential for receptor activation and cellular signaling, Cell Signal 22(2) 314-24.

3. Arabkhari M, Bunda S, Wang Y, Wang A, Pshezhetsky A V and Hinek A, (2010) Desialylation of insulin receptors and IGF-1 receptors by neuraminidase-1 controls the net proliferative response of L6 myoblasts to insulin, Glycobiology 20(5) 603-16.
4. Atanasova M, Konova E, Georgieva M, Dimitrova A, Coquand-Gandit M, Faury G and Baydanoff S, (2010) Age-related changes of anti-elastin antibodies in senescence-accelerated mice, Gerontology 56(3) 310-8.
5. Bennasroune A, Romier-Crouzet B, Blaise S, Laffargue M, Efremov R G, Martiny L, Maurice P and Duca L, (2019) Elastic fibers and elastin receptor complex: Neuraminidase-1 takes the center stage, Matrix Biol 84 57-67.
6. Blaise S, Romier B, Kawecki C, Ghirardi M, Rabenoelina F, Baud S, Duca L, Maurice P, Heinz A, Schmelzer C E, Tarpin M, Martiny L, Garbar C, Dauchez M, Debelle L and Durlach V, (2013) Elastin-derived peptides are new regulators of insulin resistance development in mice, Diabetes 62(11) 3807-16.
7. Blanchevoye C, Floquet N, Scandolera A, Baud S, Maurice P, Bocquet O, Blaise S, Ghoneim C, Cantarelli B, Delacoux F, Dauchez M, Efremov R G, Martiny L, Duca L and Debelle L, (2012) Interaction between the elastin peptide VGVAPG and human elastin binding protein, J Biol Chem 288(2) 1317-28.
8. Bocquet O, Wahart A, Sarazin T, Vincent E, Schneider C, Fougerat A, Gayral S, Henry A, Blaise S, Romier-Crouzet B, Boulagnon C, Jaisson S, Gillery P, Bennasroune A, Sartelet H, Laffargue M, Martiny L, Duca L and Maurice P, (2021) Adverse Effects of Oseltamivir Phosphate Therapy on the Liver of LDLR-/- Mice Without Any Benefit on Atherosclerosis and Thrombosis, J Cardiovasc Pharmacol 77(5) 660-672.
9. Chou C Y, Hsu D Y and Chou C H, (2023) Predicting the Onset of Diabetes with Machine Learning Methods, J Pers Med 13(3).
10. Czech M P and Massague J, (1982) Subunit structure and dynamics of the insulin receptor, Fed Proc 41(11) 2719-23.
11. Debelle L, Alix A J, Jacob M P, Huvenne J P, Berjot M, Sombret B and Legrand P, (1995) Bovine elastin and kappa-elastin secondary structure determination by optical spectroscopies, J Biol Chem 270(44) 26099-103.
12. Debelle L and Tamburro A M, (1999) Elastin: molecular description and function, Int J Biochem Cell Biol 31(2) 261-72.
13. Dridi L, Seyrantepe V, Fougerat A, Pan X, Bonneil E, Thibault P, Moreau A, Mitchell G A, Heveker N, Cairo C W, Issad T, Hinek A and Pshezhetsky A V, (2013) Positive regulation of insulin signaling by neuraminidase 1, Diabetes 62(7) 2338-46.
14. Fougerat A, Pan X, Smutova V, Heveker N, Cairo C W, Issad T, Larrivee B, Medin J A and Pshezhetsky A V, (2018) Neuraminidase 1 activates insulin receptor and reverses insulin resistance in obese mice, Mol Metab 12 76-88.
15. Guillot A, Dauchez M, Belloy N, Jonquet J, Duca L, Romier B, Maurice P, Debelle L, Martiny L, Durlach V, Baud S and Blaise S, (2016) Impact of sialic acids on the molecular dynamic of bi-antennary and tri-antennary glycans, Sci Rep 6 35666.
16. Guo T, Datwyler P, Demina E, Richards M R, Ge P, Zou C, Zheng R, Fougerat A, Pshezhetsky A V, Ernst B and Cairo C W, (2018) Selective Inhibitors of Human Neuraminidase 3, J Med Chem 61(5) 1990-2008.
17. Hayashida K, Bartlett A H, Chen Y and Park P W, (2010) Molecular and cellular mechanisms of ectodomain shedding, Anat Rec (Hoboken) 293(6) 925-37.
18. Heikkinen S, Argmann C A, Champy M F and Auwerx J, (2007) Evaluation of glucose homeostasis, Curr Protoc Mol Biol Chapter 29 Unit 29B 3.
19. Hocine T, Blaise S, Hachet C, Guillot A, Sartelet H, Maurice P, Bennasroune A, Martiny L, Duca L, Romier-Crouzet B and El Btaouri H, (2020) Lactosylceramide induced by elastin-derived peptides decreases adipocyte differentiation, J Physiol Biochem 76(3) 457-467.
20. Issad T, Tavare J M and Denton R M, (1991) Analysis of insulin receptor phosphorylation sites in intact rat liver cells by two-dimensional phosphopeptide mapping. Predominance of the tris-

phosphorylated form of the kinase domain after stimulation by insulin, Biochem J 275 (Pt 1)(Pt 1) 15-21.
21. Kawecki C, Hezard N, Bocquet O, Poitevin G, Rabenoelina F, Kauskot A, Duca L, Blaise S, Romier B, Martiny L, Nguyen P, Debelle L and Maurice P, (2015) Elastin-derived peptides are new regulators of thrombosis, Arterioscler Thromb Vasc Biol 34(12) 2570-8.
22. Kim W J, Lee W, Jung Y, Jang H J, Kim Y K and Kim S N, (2019) PPARbeta/delta agonist GW501516 inhibits TNFalpha-induced repression of adiponectin and insulin receptor in 3T3-L1 adipocytes, Biochem Biophys Res Commun 510(4) 621-628.
23. Mammoto A, Matus K and Mammoto T, (2022) Extracellular Matrix in Aging Aorta, Front Cell Dev Biol 10 822561.
24. Maurice P, Baud S, Bocharova O V, Bocharov E V, Kuznetsov A S, Kawecki C, Bocquet O, Romier B, Gorisse L, Ghirardi M, Duca L, Blaise S, Martiny L, Dauchez M, Efremov R G and Debelle L, (2016) New Insights into Molecular Organization of Human Neuraminidase-1: Transmembrane Topology and Dimerization Ability, Sci Rep 6 38363.
25. Pan J, Kothan S, Liu L, Moe A T M, Dong L, Sun Y and Yang Y, (2021) Autophagy participants in the dedifferentiation of mouse 3T3-L1 adipocytes triggered by hypofunction of insulin signaling, Cell Signal 80 109911.
26. Papa V, Russo P, Gliozzo B, Goldfine I D, Vigneri R and Pezzino V, (1993) An intact and functional soluble form of the insulin receptor is secreted by cultured cells, Endocrinology 133(3) 1369-76.
27. Pezzino V, Papa V, Costantino A, Frittitta L, Russo P, Goldfine I D and Vigneri R, (1992) Identification and initial characterization of insulin receptor-like immunoreactivity in human plasma, J Clin Endocrinol Metab 74(5) 1116-21.
28. Pierre A, Lemaire F, Meghraoui-Kheddar A, Audonnet S, Hery-Huynh S and Le Naour R, (2019) Impact of aging on inflammatory and immune responses during elastin peptide-induced murine emphysema, Am J Physiol Lung Cell Mol Physiol 316(4) L608-L620.
29. Qin Z, (2015) Soluble elastin peptides in cardiovascular homeostasis: Foe or ally, Peptides 67 64-73.
30. Reed B C and Lane M D, (1980) Insulin receptor synthesis and turnover in differentiating 3T3-L1 preadipocytes, Proc Natl Acad Sci U S A 77(1) 285-9.
31. Romier B, Dray C, Vanalderwiert L, Wahart A, Hocine T, Dortignac A, Garbar C, Garbar C, Boulagnon C, Bouland N, Maurice P, Bennasroune A, Sartelet H, Martiny L, Duca L, Valet P and Blaise S, (2021) Apelin expression deficiency in mice contributes to vascular stiffening by extracellular matrix remodeling of the aortic wall, Sci Rep 11(1) 22278.
32. Romier B, Ivaldi C, Sartelet H, Heinz A, Schmelzer C E H, Garnotel R, Guillot A, Jonquet J, Bertin E, Gueant J L, Alberto J M, Bronowicki J P, Amoyel J, Hocine T, Duca L, Maurice P, Bennasroune A, Martiny L, Debelle L, Durlach V and Blaise S, (2018) Production of Elastin-Derived Peptides Contributes to the Development of Nonalcoholic Steatohepatitis, Diabetes 67(8) 1604-1615.
33. Rosengren A and Dikaiou P, (2023) Cardiovascular outcomes in type 1 and type 2 diabetes, Diabetologia 66(3) 425-437.
34. Sasaki A, Hata K, Suzuki S, Sawada M, Wada T, Yamaguchi K, Obinata M, Tateno H, Suzuki H and Miyagi T, (2003) Overexpression of plasma membrane-associated sialidase attenuates insulin signaling in transgenic mice, J Biol Chem 278(30) 27896-902.
35. Schmelzer C E H and Duca L, (2022) Elastic fibers: formation, function, and fate during aging and disease, FEBS J 289(13) 3704-3730.
36. Soluble Insulin Receptor Study G, (2007) Soluble insulin receptor ectodomain is elevated in the plasma of patients with diabetes, Diabetes 56(8) 2028-35.
37. Sparrow L G, McKern N M, Gorman J J, Strike P M, Robinson C P, Bentley J D and Ward C W, (1997) The disulfide bonds in the C-terminal domains of the human insulin receptor ectodomain, J Biol Chem 272(47) 29460-7.
38. Sun H, Saeedi P, Karuranga S, Pinkepank M, Ogurtsova K, Duncan B B, Stein C, Basit A, Chan J C N, Mbanya J C, Pavkov M E, Ramachandaran A, Wild S H, James S, Herman W H, Zhang P, Bommer C, Kuo

S, Boyko E J and Magliano D J, (2022) IDF Diabetes Atlas: Global, regional and country-level diabetes prevalence estimates for 2021 and projections for 2045, Diabetes Res Clin Pract 183 109119.
39. Szychowski K A, Skora B, Tobiasz J and Gminski J, (2020) Elastin-derived peptide VGVAPG decreases differentiation of mouse embryo fibroblast (3T3-L1) cells into adipocytes, Adipocyte 9(1) 234-245.
40. Talukdar S, Oh da Y, Bandyopadhyay G, Li D, Xu J, McNelis J, Lu M, Li P, Yan Q, Zhu Y, Ofrecio J, Lin M, Brenner M B and Olefsky J M, (2012) Neutrophils mediate insulin resistance in mice fed a high-fat diet through secreted elastase, Nat Med 18(9) 1407-12.
41. Tavare J M, O'Brien R M, Siddle K and Denton R M, (1988) Analysis of insulin-receptor phosphorylation sites in intact cells by two-dimensional phosphopeptide mapping, Biochem J 253(3) 783-8.
42. Tembely D, Henry A, Vanalderwiert L, Toussaint K, Bennasroune A, Blaise S, Sartelet H, Jaisson S, Gales C, Martiny L, Duca L, Romier-Crouzet B and Maurice P, (2022) The Elastin Receptor Complex: An Emerging Therapeutic Target Against Age-Related Vascular Diseases, Front Endocrinol (Lausanne) 13 815356.
43. Tomic D, Shaw J E and Magliano D J, (2022) The burden and risks of emerging complications of diabetes mellitus, Nat Rev Endocrinol 18(9) 525-539.
44. Toussaint K, Appert-Collin A, Morjani H, Albrecht C, Sartelet H, Romier-Crouzet B, Maurice P, Duca L, Blaise S and Bennasroune A, (2022) Neuraminidase-1: A Sialidase Involved in the Development of Cancers and Metabolic Diseases, Cancers (Basel) 14(19).
45. Wahart A, Bennasroune A, Schmelzer C H E, Laffargue M, Blaise S, Romier-Crouzet B, Sartelet H, Martiny L, Gillery L, Jaisson S, Maurice P and Duca L, (2021), Role of elastin and elastin-derived peptides in arterial stiffness : from synthesis to potential therapeutic interventions, in: Chirinos J. (Ed.), Arterial Stiffness and Pulsatile Hemodynamics in Health and Disease. pp. 299-309.
46. Wahart A, Hocine T, Albrecht C, Henry A, Sarazin T, Martiny L, El Btaouri H, Maurice P, Bennasroune A, Romier-Crouzet B, Blaise S and Duca L, (2019) Role of elastin peptides and elastin receptor complex in metabolic and cardiovascular diseases, FEBS J 286(15) 2980-2993.
47. Yoshizumi S, Suzuki S, Hirai M, Hinokio Y, Yamada T, Yamada T, Tsunoda U, Aburatani H, Yamaguchi K, Miyagi T and Oka Y, (2007) Increased hepatic expression of ganglioside-specific sialidase, NEU3, improves insulin sensitivity and glucose tolerance in mice, Metabolism 56(3) 420-9.
48. Zhang B, Tavare J M, Ellis L and Roth R A, (1991) The regulatory role of known tyrosine autophosphorylation sites of the insulin receptor kinase domain. An assessment by replacement with neutral and negatively charged amino acids, J Biol Chem 266(2) 990-6.

Table 1: Main parameters used during the molecular docking simulation.

FFT Mode	3D
Sampling method	Range Angles
Post processing	None
Grid dimension	0.6
Solutions	2000
Receptor range	180 (Step size 7.5)
Ligand range	180 (Step size 7.5)
Twist range	360 (Step size 5.5)
Distance range	40
Box size	10
Translation step	0.8

FFT, First Fourier Transform.

Table 2: Parameters used for molecular dynamics simulations.

Package	GROMACS v 5.0.2
Force field	Adapted OPLS-AA
Constraint algorithm for H-bond	LINCS
Box shape	Cubic
Box side size (nm)	18
Water model	TIP3P
Number of water molecule	200000
Duration (ns)	250
Integration time step (fs)	2
Rlist (nm)	1.5
Rcoulomb (nm)	1.5
Coulomb type	PME
PME order	4
Rvdw (nm)	1.5
Temperature coupling algorithm	v-rescale
Tau-t (ps)	0.1
Reference temperature (K)	310
Pressure coupling algorithm	Berendsen
Tau_p (ps)	4
Reference pressure (bar)	1

OPLS-AA: all-atom optimized potentials for liquid simulations; LINCS: LINear Constraint Solver; PME: Particle mesh Ewald.

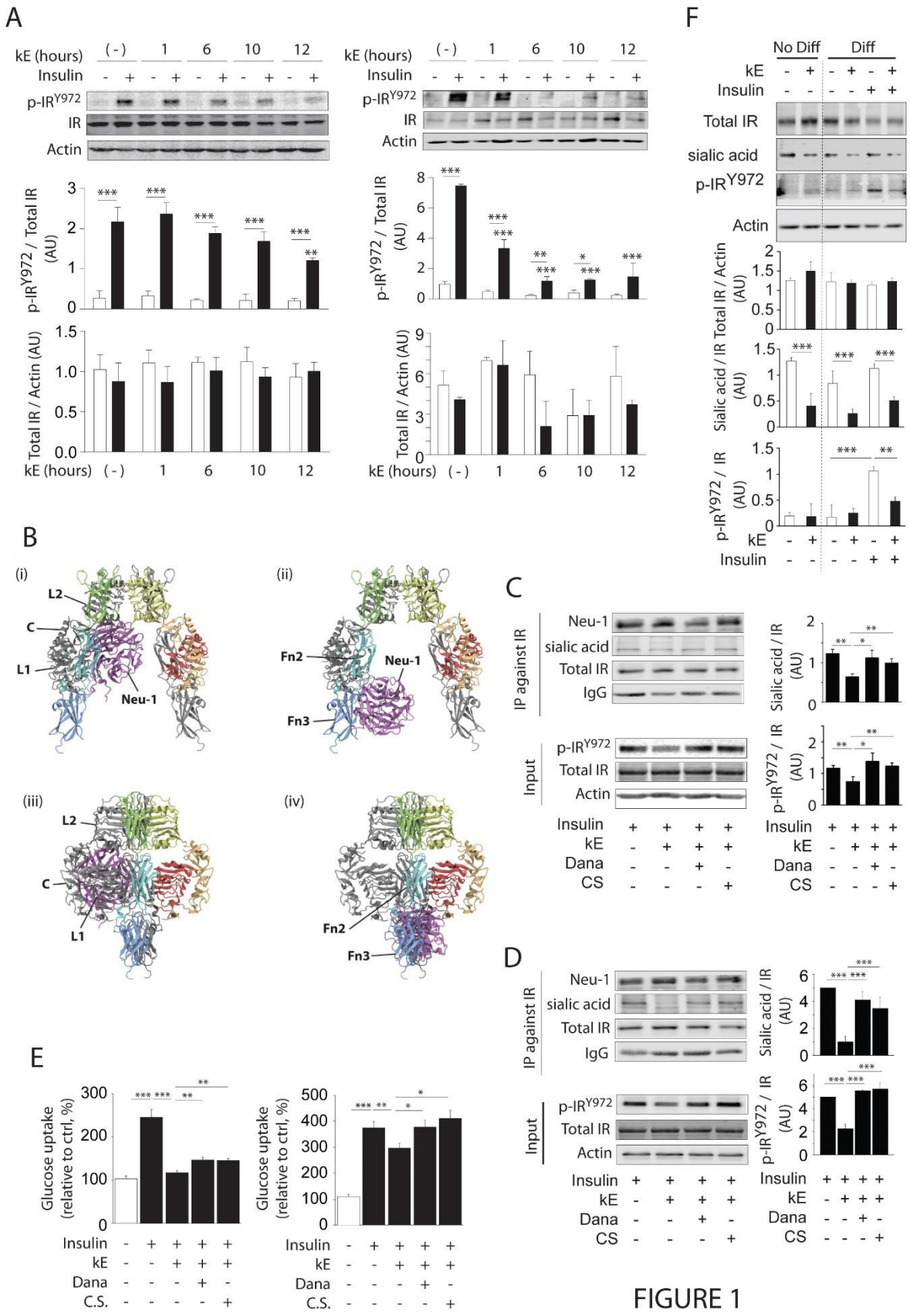

FIGURE 1

Figure 1: Elastin peptides decrease the autophosphorylation of the insulin receptor on the murine preadipocyte line 3T3-L1 differentiated or not into mature adipocyte. **A-** Western blot representing the level of, phosphorylation and native of the IR after stimulation with κE

(50 µg/mL, for 0h to 24h), associated or not with insulin (100 nM, for 30 minutes) on the preadipocytes (left panel) and mature adipocytes (right panel). The quantification of the gray levels of each blot is carried out using the Odyssey device from Li-Cor. **B-** Molecular docking simulations between Neu-1 (purple) and the IR monomer formed by leucin-rich domains (L1, red, and L2, yellow), cysteine-riche domain (C, orange), fibronectin domains (Fn1 (green), Fn2 (light blue), Fn3(dark blue)) and by insert domains (gray). Panels [i] and [ii] present a side view while panels [iii] and [iv] present a top view of the complex. Neu-1 is likely to interact with IR either at leucine 1 and 2 (L1, L2), and cysteine (C) domains - panels [i] and [iii], binding energy E = -989, 9 kcal/mol- either at the fibronectin 2 (Fn2) and 3 (Fn3) domains - panels [ii] and [iv], binding energy E = -930.1 kcal/mol. **C and D** Immunoprecipitation of IR from protein extracts from preadipocytes (C) and mature adipocytes (D) and western blot after stimulation with or without κE (50 mg/mL, 24h), in the presence or absence of chondroitin sulfate (CS) or DANA. The phosphorylated, native forms of the IR are highlighted, such as the level of sialic acids associated with the IR and the level of expression of Neu-1. **E-** Quantification of glucose uptake into preadipocytes (left panel) and mature adipocytes (right panel) after stimulation with or without κE (50 mg/mL, 24 h), in the presence or not of chondroitin sulfate (CS), DANA and/or insulin. F. Western Blot and quantification of IR sialylation in 3T3-L1 differentiated (Diff) or not (No Diff) and stimulated with kE (50 mg/mL, 24 h) and/or insulin (100 nM, for 30 minutes). Results expressed as means ± standard deviation (n = 3). ***p<0.001; **p<0.01; * p < 0.05.

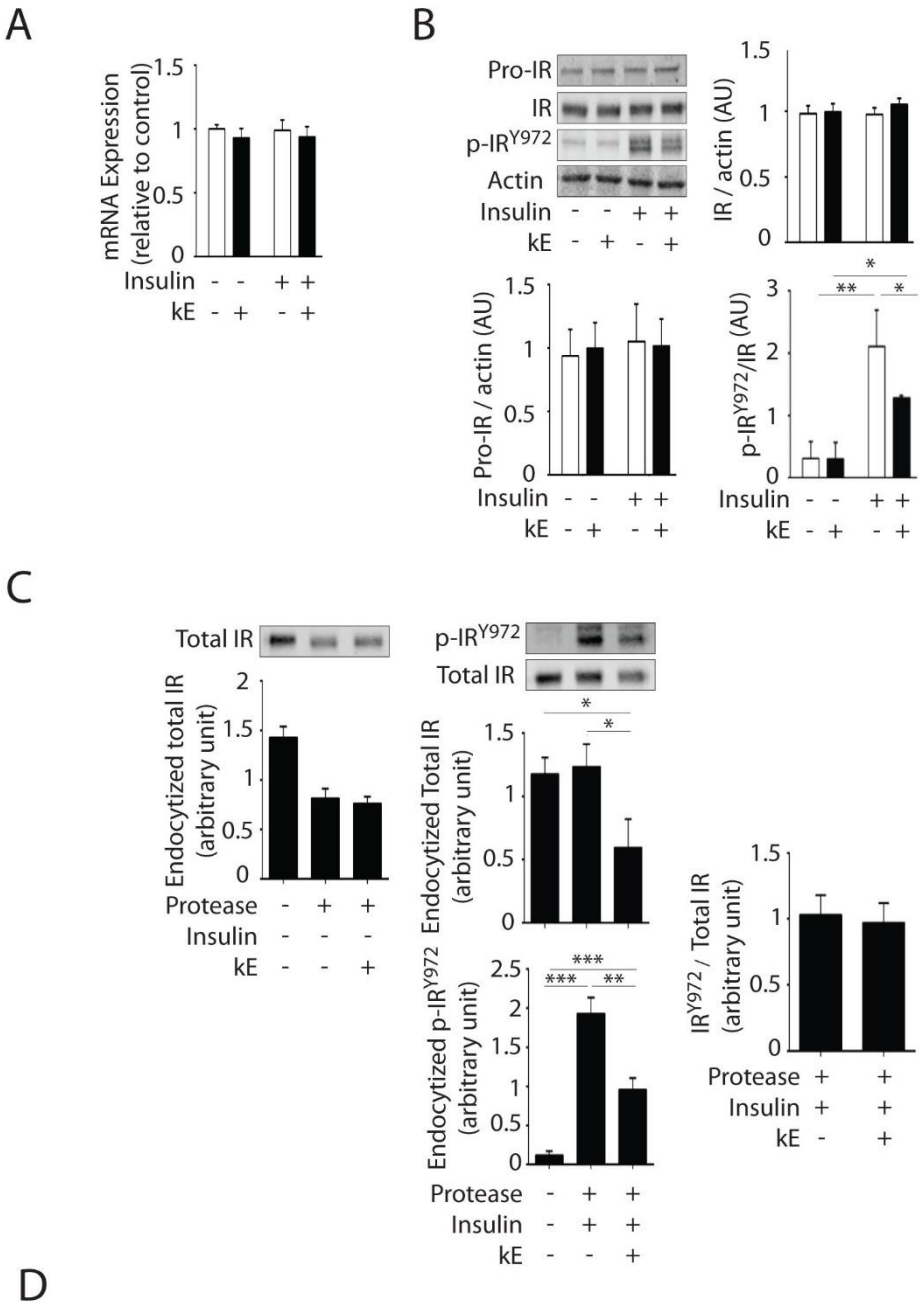
A
mRNA Expression (relative to control)
Insulin
kE
B
Pro-IR
IR
p-IR^{Y972}
Actin
IR / actin (AU)
Pro-IR / actin (AU)
p-IR^{Y972}/IR (AU)
C
Total IR
Endocytized total IR (arbitrary unit)
Protease
p-IR^{Y972}
Endocytized Total IR (arbitrary unit)
Endocytized p-IR^{Y972} (arbitrary unit)
IR^{Y972} / Total IR (arbitrary unit)
D
IR-s
IR
IR- Ctf
γ-sécrétase
Pro-IR
IR
IR-ctf
DAPT

FIGURE 2

Figure 2: Origin of insulin receptor dysfunctions induced by EDPs in preadipocytes. **A-** mRNA expression of IR obtained by qPCR. **B-** Western blot on membrane extracts after stimulation ± κE and ± insulin. Normalized results vs actin from supernatant. Results expressed as means ± standard deviation (n = 3). Statistical analyzes performed 2 by 2 vs untreated control (Ctrl Basal). **p<0.01; * p < 0.05. **C-** Analysis of the internalization of IR. The membrane proteins are biotinylated, then the cells returned to culture for 15 min, after which treatment with a protease makes it possible to eliminate the biotinylated proteins that would not have been internalized (with the exception of the positive control). Left panel represents the level of endocytosed IR without insulin stimulation. Middle panel, insulin induces phosphorylation of IR, and of its endocytosis at the level of the positive control. Right panel represents the ratio between endocytosed IR and its phosphorylated form. Results expressed as means ± standard deviation (n = 3). Statistical analyzes performed 2 by 2 vs positive control (Ctrl pos). ***p<0.001; **p<0.01; * p < 0.05. **D-** Analysis of IR shedding. The left panel illustrates the shedding process generating 2 fragments, a soluble fragment released into the extracellular medium (IR-s) and the c-terminal fragment (IR-ctf) which will be degraded by γ-secretase. The right panel is the western IR blot to identify 3 forms of the receptor (pro, mature, and c-terminal fragment). DAPT inhibits γ-secretase and therefore accumulates IR-ctf.

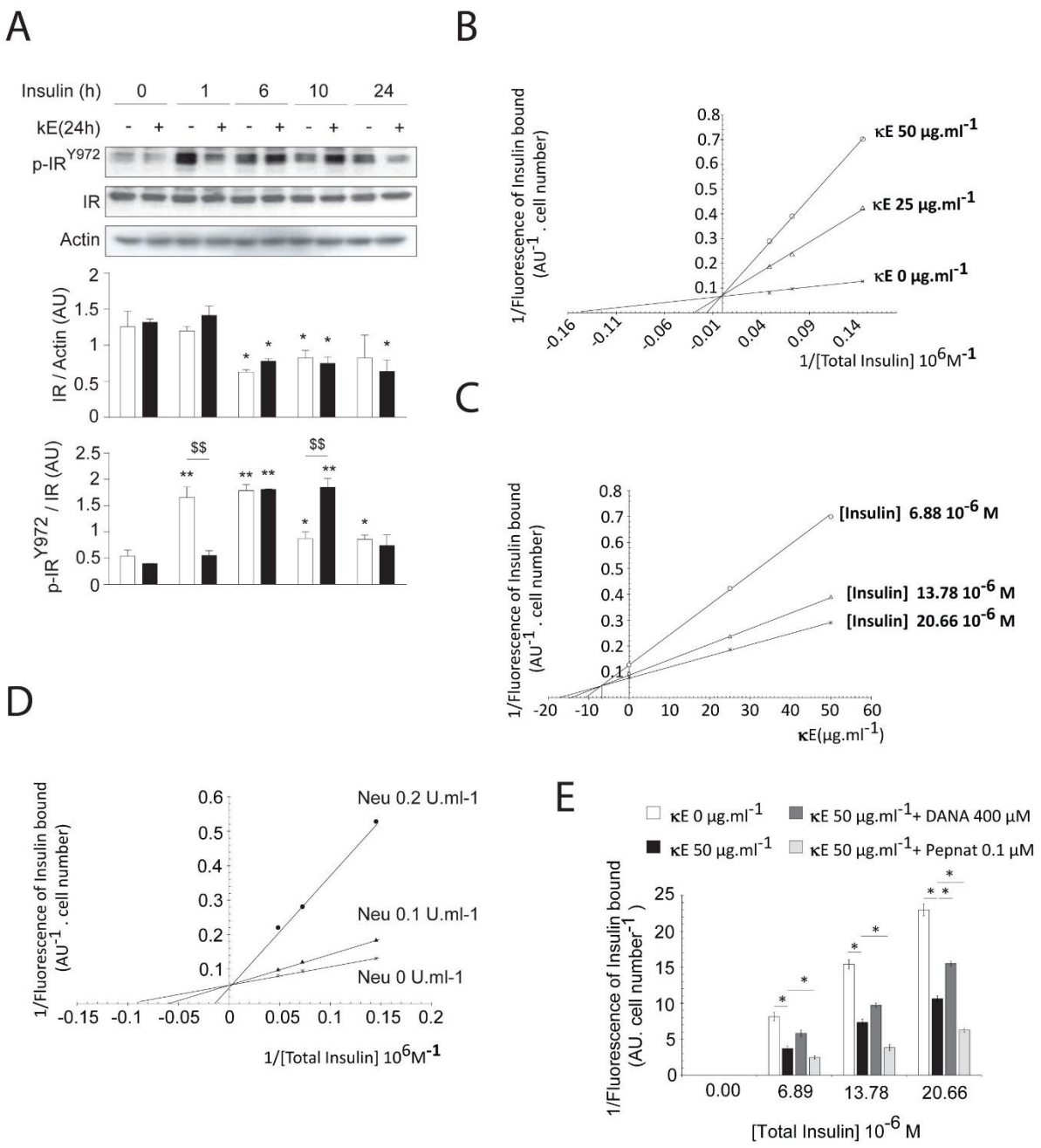

FIGURE 3

Figure 3: Desialylation induced by EDPs, decrease the affinity between insulin and IR in preadipocytes. A- Western blot representing the form of, phosphorylated and native of the IR after stimulation with insulin (100 nM, for 0 to 24h), associated or not with κE (50 µg/mL, for 24h) on preadipocytes. Results expressed as means ± standard deviation (n = 3). Statistical analyzes performed 2 by 2 vs untreated control (Ctrl Basal). **p<0.01; * p < 0.05. B- Quantification of the fluorescent insulin fraction bound to the cells after an incubation of FITC-labeled insulin (6.88, 13.78 and 20.66 10-6 M) in the presence or absence of κE (25 and 50 µg.mL^{-1} for 24h). The amount of fluorescence was related to the number of total cells contained in the well. The experiment was repeated 4 times. C- Evaluation of the κE dose effect on the interaction of insulin with its receptor using the Dixon method. Preadipocytes

are incubated for 24h with κE (25 and 50 µg.ml^{-1}) in the presence or absence of fluorochrome FITC-labeled insulin (6.88, 13.78 and 20.66 10-6 M for 30 minutes) and measured the fraction of insulin bound to the cells. **D-** Measurement of insulin bound to the preadipocytes, or absence of Bacterial neuraminidase (0.1 and 0.2 U.mL^{-1}). Cells are incubated for 30 min with increasing concentrations of fluorochrome FITC-labeled insulin (6.88, 13.78 and 20.66 10-6 M). **E-** Quantification of the fluorescence emitted by the insulin-FITC fixed on the cells according to the concentrations of insulin-FITC used for the stimulation (6.88, 13.78 and 20.66 10-6 M for 30 minutes) of a on both sides of κE (0 or 50 µg/mL for 24 h) associated with inhibitors such as DANA (400 µM for 24 h) or the interfering peptide (PepNat, 0.1 µM for 24 h). For each condition, the medium contains µM of micelle (used for the encapsulation of PepNat. The experiment was repeated 4 times.

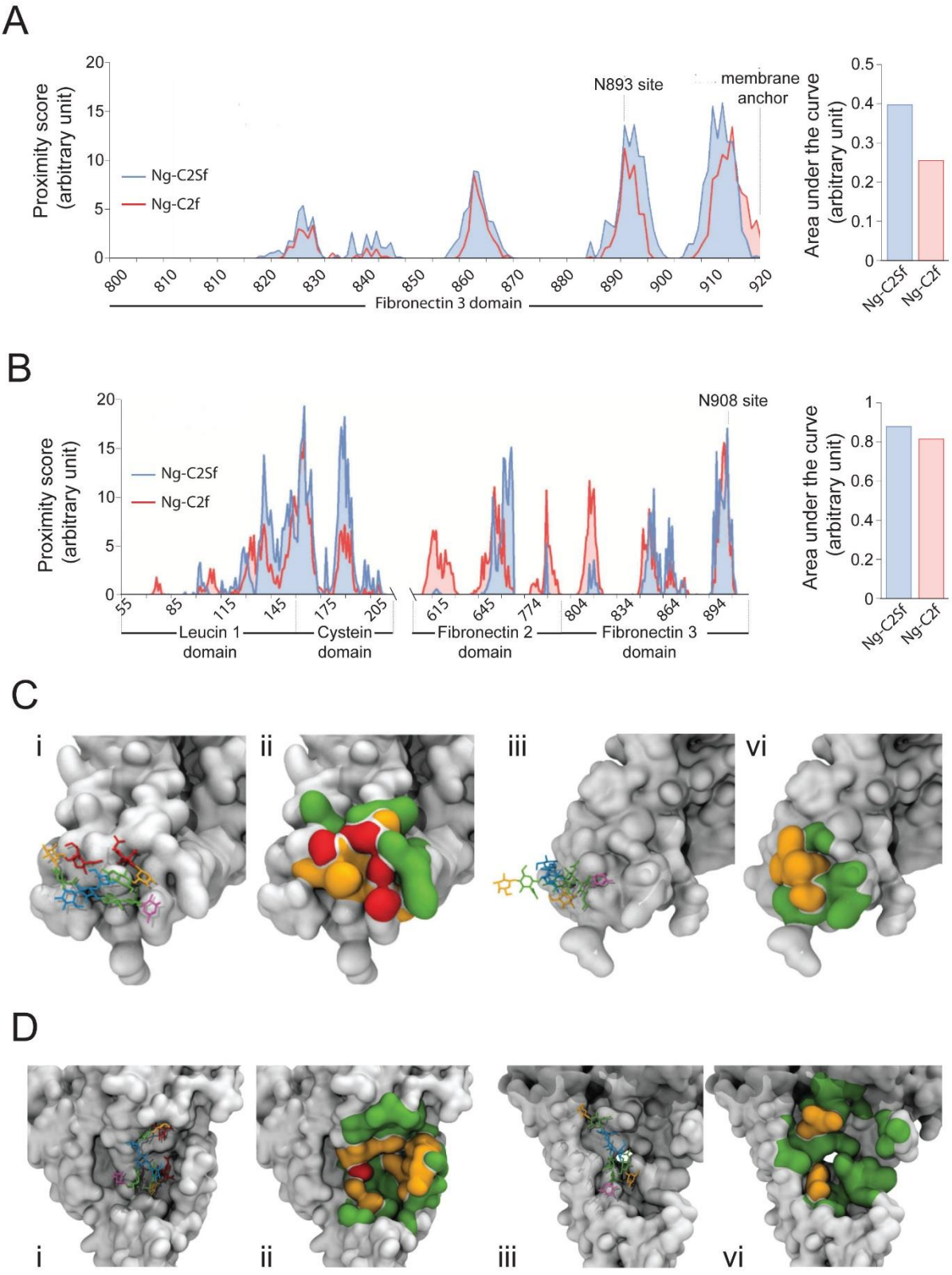

FIGURE 4

Figure 4: Desialylation of N-glycans alter their position in the pockets formed by the IR. A and B- Evaluation of the proximity score of the N-glycan chain with the residues of the insulin receptor depending on the site where it is attached: N893 (A) or N906 (B). Results associated

to chains with sialic acids (Ng-c2Sf) are represented by blue lines and areas, while results associated to chains without sialic acids (Ng-c2f) correspond to red lines and areas. **C and D-** Modifications of the position of the N-glycans upon desialylation when the N-glycosylation is on site N893 (C) or on site N906 (D). panels i and iii correspond respectively to the preferential position of the N-glycan with sialic acids (Ng-c2Sf) and without sialic acids (Ng-c2f). Panels ii and iv represent the main IR residues involved, according to the proximity scores identified in A and B (green if > 5; orange if > 10; and red if > 15). The N-glycan is displayed with the color code such as N-acetylglycosamine (green), mannose (blue), galactose (orange), fucose (purple), sialic acid (red). The insulin receptor is displayed in surface mode representation and in gray.

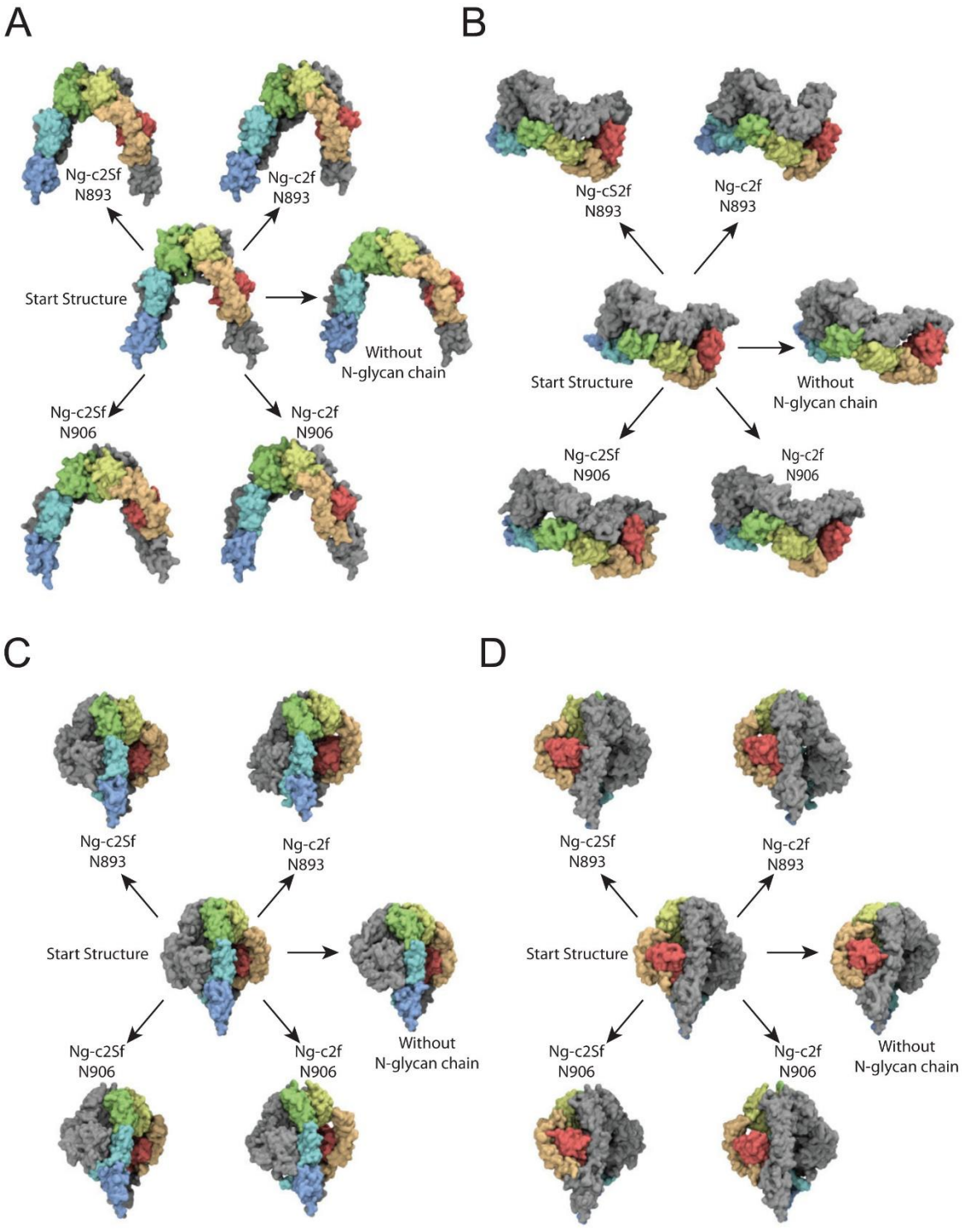

FIGURE 5

Figure 5: Conformations of IR grafted with sialylated (Ng-C2Sf) or unsialylated (Ng-C2f) N-glycan chains on asparagine residues N893 and N906. The arrows point from the starting structure toward each of the structures obtained after 250 ns of MD-simulation. A- Front view, B- from above, C and D from the side. the IR is represented using the “quick-surf” mode. The

first monomer presents the different domains forming the alpha and beta chains, colored such that the leucin-rich domains (L1 and L2) are red and orange, cysteine-riche domain (C) is orange, fibronectin domains (Fn1, Fn2, Fn3) are respectively green, light blue and dark blue. The second monomer is shown in gray.

Supplemental Methods:

Animal models: All mouse procedures are conformed to the Guide for Care and Use of Laboratory Animals of the US National Institutes of Health. The study respected European and French legislation on good practices in animal experimentation and was approved by the Animal Subjects Committee of Champagne Ardenne (CEEA-RCA-56). male C57Bl/6J mice, and male db/db mice (C57BL6/J as genetic background) are 8 weeks old in order to test the treatments. Mice were purchased from Janvier (Le Genest-Saint-Isle, France) All mice had ad libitum access to a standard diet (AIN-93 M rodent diet, Special Diet Service, UK) and water during the experimental period.

Treatments: kE (10 or 100 mg/kg) was injected in the tail vein of the mice C57/Bl6J. The ERC inhibitors, 2-deoxy-2,3-dehydro-*N*-acetylneuraminic acid (DANA, 10 g/L) and chondroitin sulfate (CS, 50 mg/kg) were injected intraperitoneally. GW311616A (sigma), a neutrophil elastase inhibitor, was injected intraperitoneally, at 2 mg/kg per day for 14 days. These three inhibitors were administered in Db/Db mice.

Serum metabolic parameters: Plasma glucose, Glucose tolerance (GTT) and insulin sensitivity (IPIST) tests were performed as reported by Heikkinen et al. ([18]) on mice fasted for 4 h.

Supplementary data:

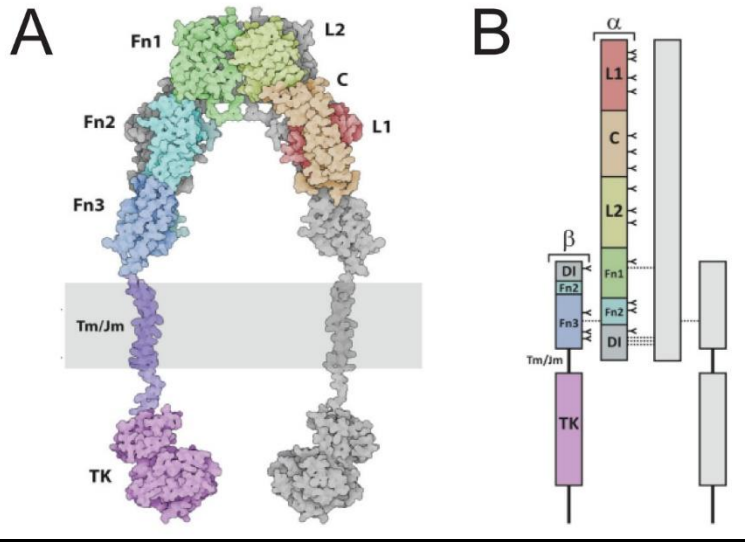

Supplemental figure 1: Structure of the insulin receptor. A- A- 3D structure of an IR homodimer assembled using the structures corresponding to 3LOH, 2MRF and 1IRK PDB ID.B- Schematic structure of the different IR domains: leucine-rich (L1 and L2), cystein-rich (C), fibronectin (Fn1, Fn2, Fn3), insertion (DI), trans- and juxtamembrane (Tm) domains /Jm), and tyrosine kinase (TK). The disulfide bridges are annotated in dotted lines and the N-glycosylation sites are displayed under the symbol “Y”.

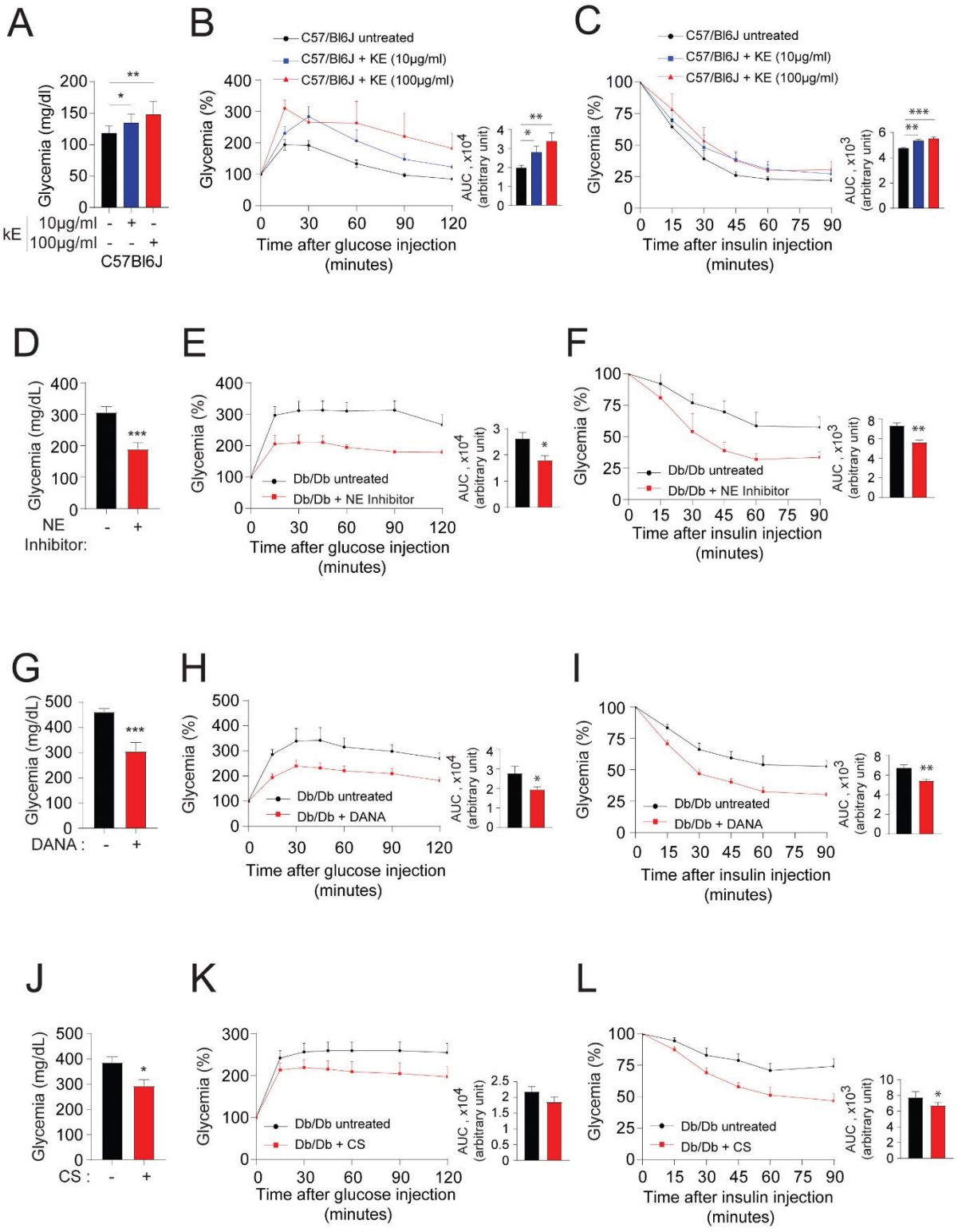

SUPPLEMENTAL FIGURE 2

Supplementary figure 2: EDPs contribute to insulin-resistance in vivo. A to C: C57/Bl6J (n=5/group) were injected with kE (10 or 100 mg/kg/once week for 8 weeks) and plasma glucose (A), GTT (B) and IPIST (C) were performed. D to F: Db/Db mice (n=5/group) were treated for 14 days with GW311616A, an inhibitor of neutrophil elastase (NE) and plasma glucose (D), GTT (E) and IPIST (F). G to I: Db/Db

mice (n=5/group) were treated for 8 weeks with DANA (10g/l) and plasma glucose (G), GTT (H) and IPIST (I). J to L: Db/Db mice were treated for 8 weeks with chondroitin sulfate (CS, 50mg/L) and plasma glucose (J), GTT (K) and IPIST (L). The results shown are the mean ± SEM. Statistically significant differences: Mann-Whitney test, ** $p< 0.001$, * $p< 0.05$.

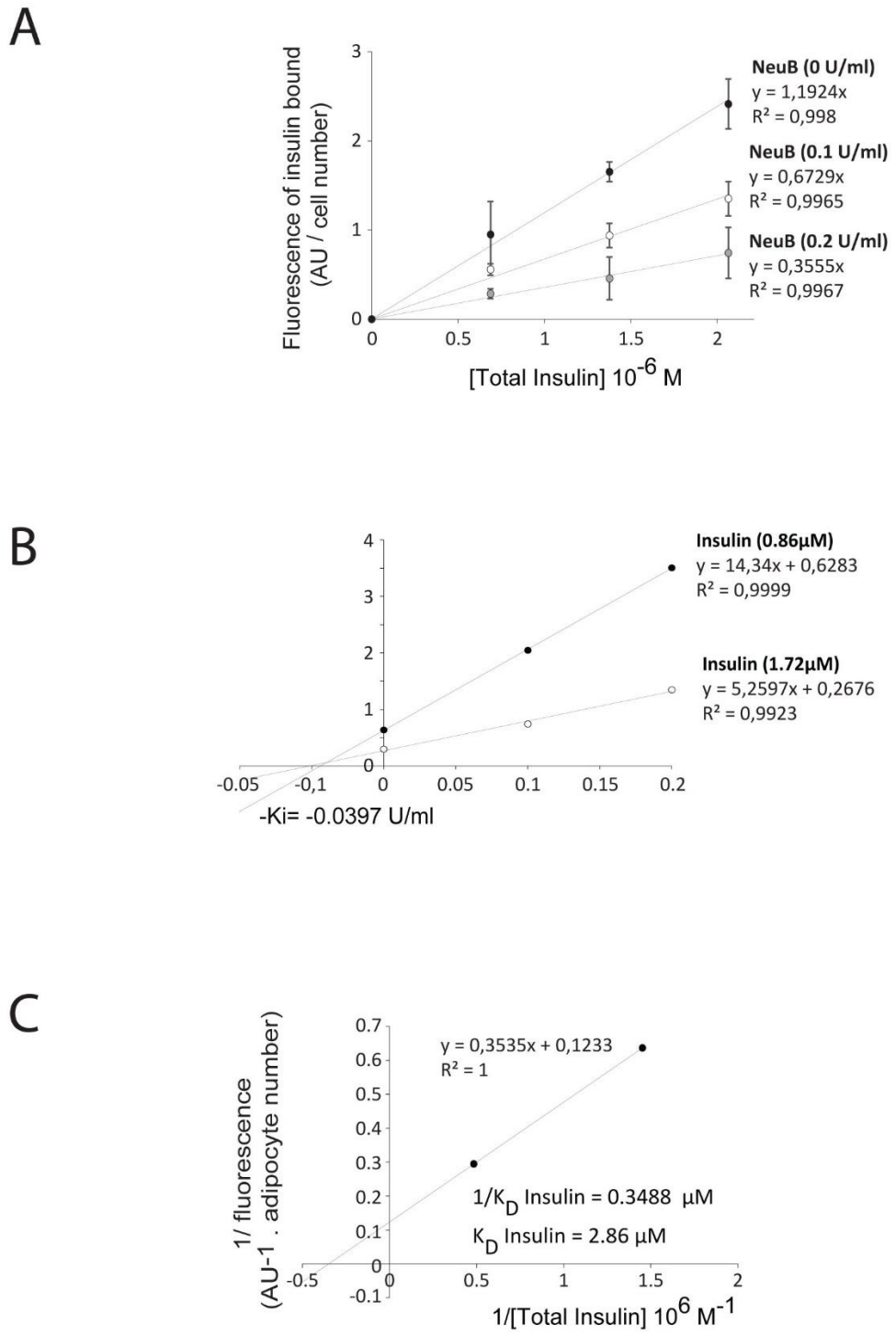

Supplementary figure 3: Impact of desialilation induced by bacterial neuraminidase (NeuB) on insulin-IR affinity in preadipocytes: A- Quantification of the fluorescence emitted by insulin-FITC fixed on the cells according to the concentrations of insulin-FITC used for stimulation (0 - 0.69 - 1.38 - 2.07 µM for 30 minutes) on the one hand and on the other hand concentrations of NeuB (0 - 0.1 - 0.2 IU/mL for 24h). was related to the number of total cells contained in the well. The experiment was repeated 4 times. B- Representation of Dixon where the fluorescence of the insulin fixed to the IR is a function of the concentration of NeuB. The cells were stimulated with 2 doses of insulin (0 - 0.1 - 0.2 IU/mL for 24 h). The intersection of the two straight lines made it possible to determine the inhibition constant of NeuB on the binding of insulin - IR (Ki). C- A secondary graph was made from the Dixon plot (panel B) to determine the dissociation constant (KD) of insulin at its receptor.

946 Supplemental Data : **Presentation of western blot (full membranes)**

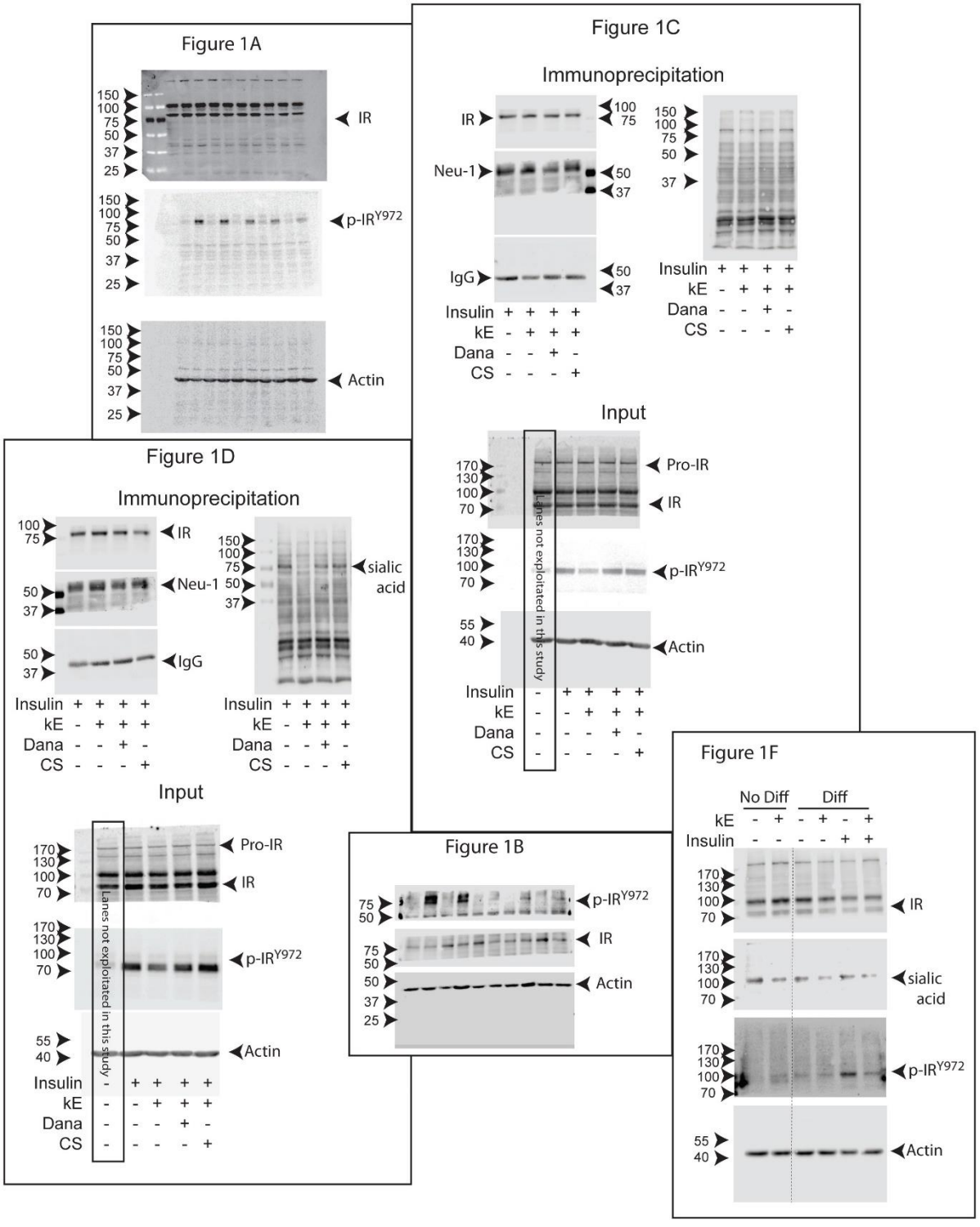

947

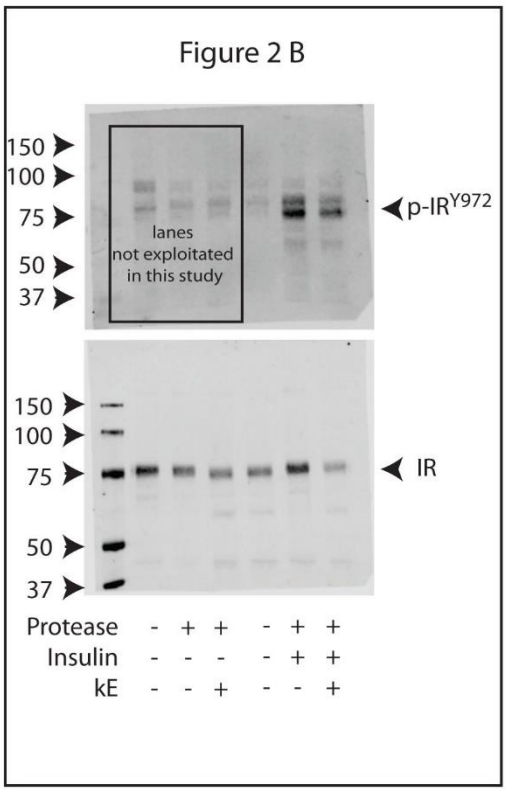
Figure 2 B
150
100
75
50
37
lanes
not exploitated
in this study
p-IR^{Y972}
150
100
75
50
37
IR
Protease - + + - + +
Insulin - - - - + +
kE - - + - - +

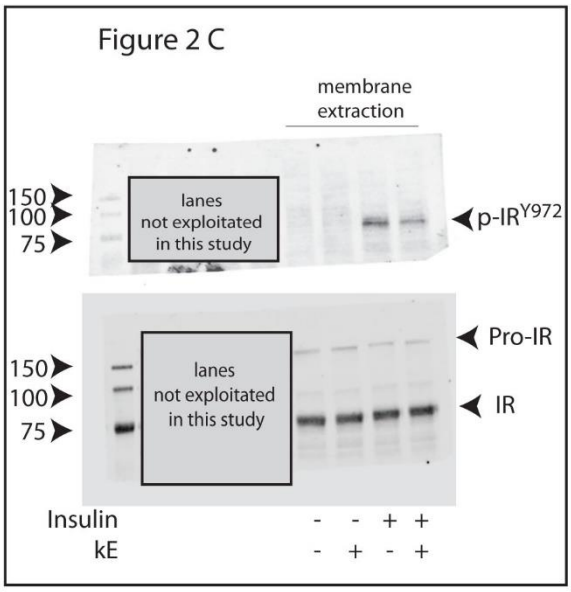
Figure 2 C
membrane
extraction
150
100
75
lanes
not exploitated
in this study
p-IR^{Y972}
Pro-IR
150
100
75
lanes
not exploitated
in this study
IR
Insulin - - + +
kE - + - +

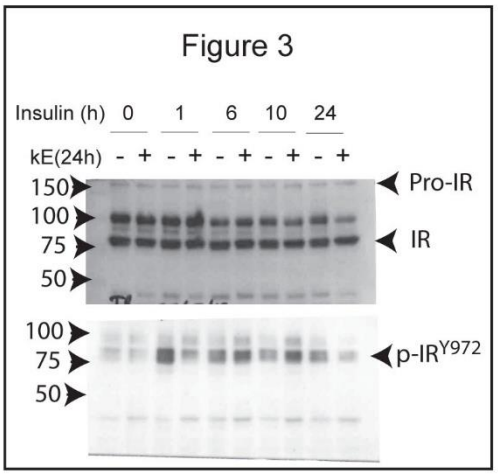
Figure 3
Insulin (h) 0 1 6 10 24
kE(24h) - + - + - + - + - +
150
100
75
50
Pro-IR
IR
100
75
50
p-IR^{Y972}

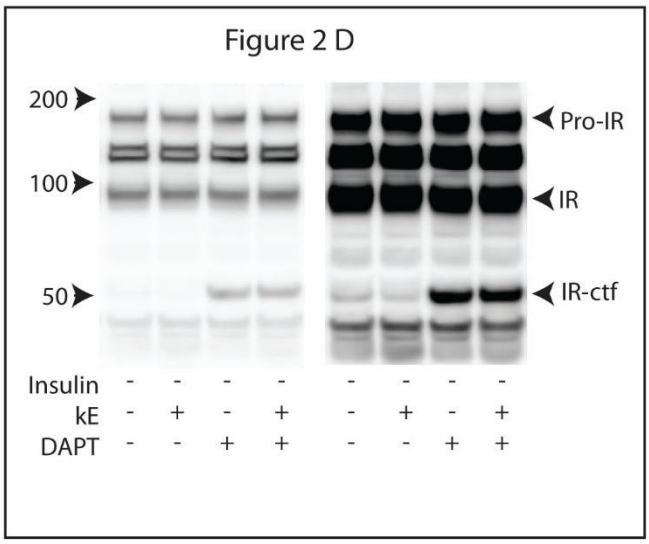
Figure 2 D
200
100
50
Pro-IR
IR
IR-ctf
Insulin - - - - - - - -
kE - + - + - + - +
DAPT - - + + - - + +

948